1-1-2018

Transient Seepage in a Variably Saturated Levee: Laboratory Testing, Field Monitoring and Numerical Modeling

Xavier Arnaldo Rivera-Hernandez

Transient seepage in a variably saturated levee: laboratory testing, field monitoring and numerical modeling

By

Xavier Arnaldo Rivera-Hernandez

A Thesis
Submitted to the Faculty of
Mississippi State University
in Partial Fulfillment of the Requirements
for the Degree of Master of Science
in Civil Engineering
in the Department of Civil and Environmental Engineering

Mississippi State, Mississippi

December 2018

Transient seepage in a variably saturated levee: laboratory testing, field monitoring and numerical modeling

By

Xavier Arnaldo Rivera-Hernandez

Approved:

_____

Farshid Vahedifard
(Major Professor/Graduate Coordinator)

_____

Ghada Ellithy
(Committee Member)

_____

Isaac L. Howard
(Committee Member)

_____

Jason M. Keith
Dean
Bagley College of Engineering

Name: Xavier Arnaldo Rivera-Hernandez

Date of Degree: December 14, 2018

Institution: Mississippi State University

Major Field: Civil Engineering

Major Professors: Dr. Farshid Vahedifard

Title of Study: Transient seepage in a variably saturated levee: laboratory testing, field monitoring and numerical modeling

Pages in Study: 67

Candidate for Degree of Master of Science

Several hydraulic loadings impose earthen levees to time-dependent variably saturated seepage conditions. The main objective of this study is to improve the analysis of levees under transient seepage with the use of unsaturated soil mechanics. An extensive set of laboratory testing, field monitoring and numerical modeling are performed to analyze a silty sand setback levee located near Seattle, WA. In-situ data obtained from field monitoring are used to monitor suction and effective stress within the levee's embankment and foundation over the past two years. Soil samples taken from the site are used to perform index, water retention, and unsaturated multi-stage triaxial tests in the laboratory. A finite element model of transient seepage under saturated-unsaturated conditions is then developed and calibrated to reasonably match the field data. The results highlight the need to consider unsaturated soil mechanics along with climatic variables and soil-atmosphere interaction when analyzing levees under transient seepage conditions.

DEDICATION

I dedicate this research to my parents and teachers. Moral values and education should always be together in this journey called life. Parental love is the only love that is truly selfless, unconditional and forgiving. Eva Luz Hernandez-Colon (mom) passed away in May 2009, from that moment I dedicated her all my success. She taught me to always be humble and kind.

Thank you Jorge David Rivera-Berrios (dad) and Jorge David Rivera-Hernandez (brother) for always being there during good and bad moments. I earnestly feel that without their inspiration, able guidance, dedication, and moral values, I would not have been able to pass through the process of this research.

ACKNOWLEDGEMENTS

The author would like to acknowledge Dr. Farshid Vahedifard and Dr. Ghada Ellithy for serving as mentors. Without their support, it would have been impossible for me to complete this thesis.

First of all, I would like to acknowledge Dr. Vahedifard, for giving me the opportunity to do research under his supervision. His support and encouragement to continue focusing during all my graduate studies helped me a lot, specifically during hard times. Secondly, I would like to thank my committee member, and friend, Dr. Ghada Ellithy for her motivation and support during the entire time. Her commitment and dedication even during the weekends was always present. Also, I would like to thank Dr. Howard for serving as one of the graduate committee and accepting being part of this work.

Special thanks to the U.S. Army Engineer Research and Development Center (ERDC) and the Civil Works program for sponsoring this research. The author would like to thank Dr. Maureen Corcoran, Chad Gartrell, and Chris Price for their continuous support of this study. Special thanks to the laboratory technician, Joseph Bonelli, for his help during this study and his positive vibe working together to find a solution to every problem encounter.

Also, special thanks to my girlfriend Dailyn Gomez-Serrano and her son Yosuel Lopez-Gomez for their unconditional support, inspiration and love.

TABLE OF CONTENTS

LIST OF TABLES

LIST OF FIGURES

CHAPTER I

INTRODUCTION

1.1 Overview

Earthen levees form a critical component of the nation's infrastructure system (NRC 2012). Over 160,000 km of earth levees provide flood protection in the U.S. (CRS 2011) and their performance and reliability are crucial for homeland safety. Levee failures can cause catastrophic damage and loss of life, as seen in the Midwest and along the Mississippi River and in New Orleans during Hurricane Katrina in 2005. The majority of the nation's existing levee infrastructure is now past its reasonable design life, and the long-term sustainability of the network is a critical issue (ASCE, 2017). Moreover, unprecedented events like rising sea levels, ground subsidence and increasing storm severity resulting from global climate change are raising the level of stress on levees (e.g., NRC 2012; Vahedifard et al., 2016a, 2018). These facts altogether highlight the need to continuously improve the state of the practice for monitoring and analyses of levees under various loading conditions.

Several short-duration and extreme hydraulic loadings impose earthen levees to time-dependent variably saturated seepage conditions. Transient seepage in variably saturated earth structures (e.g., levees, earthen dams) is a complex phenomenon due to temporal and spatial hydro-mechanical interactions in a 3-phase air-fluid-solid system. The intrinsic complexity of transient seepage under various flux boundary conditions warrants

using an advanced numerical method such as the finite element method to perform a fully coupled seepage-stability analysis. However, the level of expertise as well as several required input parameters have prevented the widespread use of numerical models in the common geotechnical engineering practice. Difficulty to assign appropriate input parameters and boundary conditions, and a lack of practical guidelines are among the main factors that have hindered the widespread application of numerical transient seepage analyses. Further, practicing engineers, in some cases, undermine the validity and accuracy of such numerical analyses due to lack of full-scale validation of the results and poor connection to field monitoring data.

The majority of earthen structures, including earthen levees, are comprised of unsaturated soils (e.g., Fredlund and Rahardjo 1993; Lu and Likos 2004). Thus, employing unsaturated soil mechanics in the analyses of earthen levees can enhance the state of practice regarding the assessment of levees during their service life. The mechanics of unsaturated soils has been studied for over four decades (e.g., Fredlund and Morgestern 1977; Fredlund and Rahardjo 1993; Lu and Likos 2004). Major research advances have been made in several areas including definition and measurement of stress state variables, factors affecting key engineering parameters (e.g., soil-water retention curve, strength, compressibility), numerical and analytical modeling, laboratory testing, and field monitoring of unsaturated soils (e.g., Lu and Likos 2004; Fredlund et al., 2012; Briaud 2013; Ng and Menzies 2014). These researches have significantly improved the state of the art about the engineering behavior of unsaturated soils. However, such research advances have not been fully adopted in the practice.

This study is an attempt to address some of the above-mentioned gaps in the state of practice on the analyses of earthen levees subjected to transient unsaturated-saturated seepage conditions. Best practices needs new guidelines to provide instructions for where and when transient seepage can be applied in an effective and correct manner due to the uncertainty and inexperience of practicing engineers. The U.S Army Corps of Engineers (USACE) is responsible for analysis, monitoring and maintaining the largest network of the nation's levee systems. The major guidance documents used for seepage analysis of levees and dams by the USACE are Engineer Manual (EM) 1110-2-1901 (USACE, Rev1993) and EM 1110-2-1913 (USACE, Rev2000). Although these EMs acknowledge the existence of transient seepage conditions, they do not provide any guidance regarding the use of transient unsaturated analyses in the engineering practice.

1.2 Objectives and Scope

The main objective of this study is to improve the analysis of levees under transient seepage with the use of unsaturated soil mechanics. An extensive set of laboratory testing, field monitoring and numerical modeling are performed to analyze a silty sand setback levee located near Seattle, WA. The levee is a part of the Qwuloolt Project, one of the nation's largest ecosystem restoration projects, which includes restoration of approximately 162 hectares of estuarine land. The project site is located about 64 kilometers north of Seattle, WA. As part of this project, a 1,219-meter-long setback levee was constructed using silty sand in 2014 to protect an industrial area behind it, while allowing for the site to be inundated with the Puget Sound water. This levee was

constructed of highly compacted silty sand material that was engineered using silt and gravelly sand material available in nearby sites.

The laboratory testing part of the study primarily focuses on multistage and single-stage triaxial testing of highly compacted unsaturated soil samples taken from the levee. This case study levee was constructed of highly compacted silty sand that was engineered using silt and gravelly sand material available in nearby sites. The silty sand was highly compacted and achieved a porosity (n) of 0.2 (void ratio e of 0.25). A modified unsaturated triaxial test equipment is used to test the shear strength response of the soil under different confining pressures and matric suction levels. Triaxial tests are commonly performed on three to four samples from the same soil depth and consolidated at different stress levels. However, in some projects, retrieving identical samples at the same depths is not possible and that is where multi-stage triaxial testing can become a viable option. In addition, if samples are limited for a specific project, multistage testing is recommended to reduce costs and time. In this work, a set of single stage and multi-stage triaxial testing are performed on high compacted silty sand samples. A testing procedure for multi-stage testing of unsaturated soil is proposed that can help toward the development of a standardized procedure for multistage triaxial testing on unsaturated soils. New features of this part of the study include experimental techniques to run multistage triaxial tests on highly compacted unsaturated soils and presentation of an equivalency between multistage and single-stage tests.

The second focus area of this study is to demonstrate how to effectively integrate field monitoring data into numerical modeling of transient seepage to evaluate the

performance of the levee under climatic and tidal variations. Filed monitoring is performed using an array of tensiometers and soil moisture sensors installed within the levee's embankment and foundation. A near real-time data acquisition system is employed to process the field data from various sensors over the past two and half years. Climatic and weather data including precipitation, temperature, humidity and solar radiation are collected from a weather station at the site whereas tidal water fluctuations are monitored using a water level sensor. The data collected from the sensors are used to monitor suction stress and effective stress versus time. A finite element model of transient seepage under saturated-unsaturated conditions is then developed and calibrated to reasonably match the measured pore water pressures and the piezometric surface, while illustrating which variables analyses are sensitive that can be used to estimate the transient seepage results. The calibrated numerical model is used in a set of parametric study.

1.3 Structure of Thesis

This thesis is divided into four chapters. Chapter 1 provides an overview, main objective and scope of this research. Chapter 2 presents results of laboratory testing to study the shear strength of highly compacted silty sand from the levee site using single-stage and multistage triaxial testing. This chapter will cover discussion on highly compacted materials, single versus multistage information and procedures and techniques for multistage triaxial testing on unsaturated soils.

Chapter 3 presents results of integrating field monitoring and numerical analysis to evaluate the performance of the earthen levee under climatic and tidal variations. This chapter will cover the background in transient seepage analysis, the need for guideline in

how to run a transient seepage model by practitioner engineers, and the importance to include the climate boundary conditions into the seepage analysis for better representation of field conditions. Chapter 4 provides the conclusions and recommendation for future works.

CHAPTER II

SATURATED AND UNSATURATED SHEAR STRENGTH OF A HIGHLY COMPACTED SILTY SAND

2.1 Introduction and Background

During the last decades, unsaturated soil mechanics has shown relevance and significance in foundation engineering, slope stability of earthen embankments such as dams and levees, underground pipelines, retaining structures, pavements and in geo-environmental engineering, and mining engineering (Shen 2013). These structures are typically constructed using compacted engineered soils. With the availability of high efficiency modern compaction equipment and techniques, most earthen structures are highly compacted and exceed the project design specifications. Such highly compacted engineered soils used in roadways and embankments stay unsaturated most of the time. Levee and dam embankments are made of compacted or highly compacted materials that can experience accumulated deformation under cyclic wetting and drying (i.e. precipitation and drought periods), which affects their serviceability (Alonso 2006).

There is limited information about the shear strength of highly compacted unsaturated soils which is important in evaluating the stability of the earthen structures which they are comprised of. It is known that highly compacted sands have a dilative behavior during shearing. Houlsby 1991 mentioned that the magnitude of the dilation depends very strongly on the density of the soil, with denser samples expanding more

rapidly. The fact that a soil is dilating has an important effect on the solutions to problems where the soil is heavily constrained. There are still challenges on how to properly understand soils that are highly compacted and dilative, which is the main reason in studying these engineered soils.

Khosravi et al. (2011) presented multistage triaxial testing to estimate the effective stress relationships for unsaturated compacted soils. A soil mixture of mortar and Bonny silt was used to demonstrate the capabilities of the multistage testing technique. The soil mixture is classified as SM according to the USCS. The soil specimen was compacted to a maximum unit density of 18.1 kN/m^3 (115 lb/ft^3), a void ratio of 0.44, and an optimum water content of 12%. Before performing the multistage triaxial testing, a series of consolidated-undrained triaxial tests with pore pressure measurements were performed on saturated soil specimens under effective stresses of 50, 100, 150, and 200 kPa. They found that the results from the multistage triaxial tests interpreted using a value of χ equal to the degree of saturation corresponded well with the critical state line obtained from independent tests on saturated specimens of the same soil. They concluded that even there are potential changes in soil structure in the specimen during loading, unloading, and reloading, the results indicate that the multistage testing method may be useful for estimating the soil-specific effective stress parameters for compacted soils in unsaturated conditions.

Benerjee et al. (2018) presented a new approach that was validated by comparing the results obtained from multistage triaxial tests and those from single-stage triaxial tests varying suction states under drained conditions. The soil used in this study is classified as

Lean silt (ML) per the USCS from a site near the Red River in Denison, Texas. The maximum dry density of the soil obtained from Proctor tests was 1.7 g/cm^3 (106.13 pcf) at an optimum moisture content of 16%. Some additional properties of the compacted specimens were a void ratio (e = 0.60), porosity (n = 0.37), and a degree of saturation (S_r = 71%). Each multistage test was performed on an isotropically consolidated specimen at a constant matric suction (s =0 or 50 kPa) and varying net confining pressures of 100, 200, and 400 kPa. Their results showed variation from 5% to 12% of the multistage compared from the conventional single triaxial test results over a varying suction range.

Patil et al. (2018) performed a series of hydrostatic compression, consolidated drained, and single stage triaxial compression tests on statically compacted specimens of unsaturated silty sand (SM) under suction-controlled conditions. They used the Barcelona basic model (BBM) to experimentally calibrated and used for prediction of the compacted silty sand response at matric suction states. The maximum dry unit density of the soil is 1.8 g/cm^3 (112.4 lb/ft^3) at an optimum water content of 14.2% (2% more than the optimum). Some additional properties of compacted specimens were an initial void ratio between 0.46 and 0.49, and a degree of saturation of 81%. The soil specimens were 71.2 mm (2.8 in) diameter and 142.24 mm (5.6 in) in height. The experimental program constituted of a fully automated double-walled triaxial test system, via the axis translation technique, for matric suctions varying from 50 to 750 kPa. The net confining pressures varied from 100 and 300 kPa. Patil et al found that the predicted values of deviatoric stress at critical state are reasonably close to those experimentally assessed from the suction controlled conventional

triaxial compression tests; however giving that the test soil had a brittle and dilatant nature, the post peak softening behavior was not adequately captured by the model.

Tripathy and Cleall (2018) explored the impact of net confining stress and suction on the volume change and shear strength behavior of collapsible soil. The triaxial shear tests were conducted in saturated and an unsaturated conditions. Consolidated drained tests were performed at confining pressures of 100, 250, and 400 kPa. The matric suction varied from 300 kPa to 0 kPa. The soil used in this study was a mix of M400 silt (40%), Leighton Buzzard sand (40%) and 20% Speswhite Kaolin. Their results shown an increased in peak strength with an increase in matric suction and confining pressures. With an increase in the applied suction, the failure envelopes on the Mohr coulomb circle for the unsaturated soil specimen were shifted in an upward direction. They found that the angle of friction for a matric suction range of 0 to 300 kPa were very similar, while the cohesion values varied from 4.8 and 61 kPa for the same range of matric suction.

The objective of this study is to explore the impact of net confining pressure and matric suction on the shear strength behavior of a highly compacted dilative silty sand material. This study present procedures and techniques to conduct single and multistage triaxial test for saturated and unsaturated soils. Another focus is to study the differences in shear strength between single-stage and multistage test. The experimental results from this study add to the understanding of the shear strength behavior of a highly compacted dilative silty sand material. Innovative aspects of this paper include experimental techniques to run multistage triaxial tests on highly compacted unsaturated soils to be used by other researchers since there are no standard guidelines.

2.2 Soils Properties and Specimen Preparation

The samples were retrieved from the study area, located in the city of Marysville, Snohomish County, Washington (Rivera-Hernandez et al. 2017). The test specimen were constituted from silty sand bulk samples retrieved from a depth of about 3 meters. The soil consisted of gravel (40.1%), sand (44.2%), and fines (15.7%). Soil specimens was sieved on 3/8-inch sieve prior to compaction and triaxial test. The soil is classified as silty sand (SM) as per the Unified Soil Classification System (USCS). From Proctor compaction tests, the maximum dry density of the soil was 21.05 kN/m^3 at an optimum moisture content of 7.2%. This density resulted in a porosity of about 0.2. Before conducting the test, each soil sample is prepared to the optimum moisture content and compacted in four layer to about 95% of the maximum dry unit weight. The soil layers were scarified after each lift for better interlocking between soil particles. The soils samples were prepared for a diameter of 50.8 mm and a height of 101.6 mm.

The soil water retention curve (SWRC) of the silty sand material was measured by running a multiple test using the Transient water Release and Imbibition Method (TRIM). Wayllace & Lu 2012 presented this new methodology to provide a fast, accurate, and simple testing tool for obtaining the SWRC for various soil types under wetting and drying states. The TRIM method uses an inverse modeling technique to develop the full curve from two matric suction (10 kPa and 95kPa) pressures that the sample is exposed.

The SWRC's shown in Figure 2.1 represent drying and wetting curves for silty sand samples retrieved from the same depth as the samples used in the triaxial test and performed on different dates. As part of running the TRIM test, a saturated hydraulic conductivity of 3.9e-05 cm/s was determined and used in obtaining the SWRC.

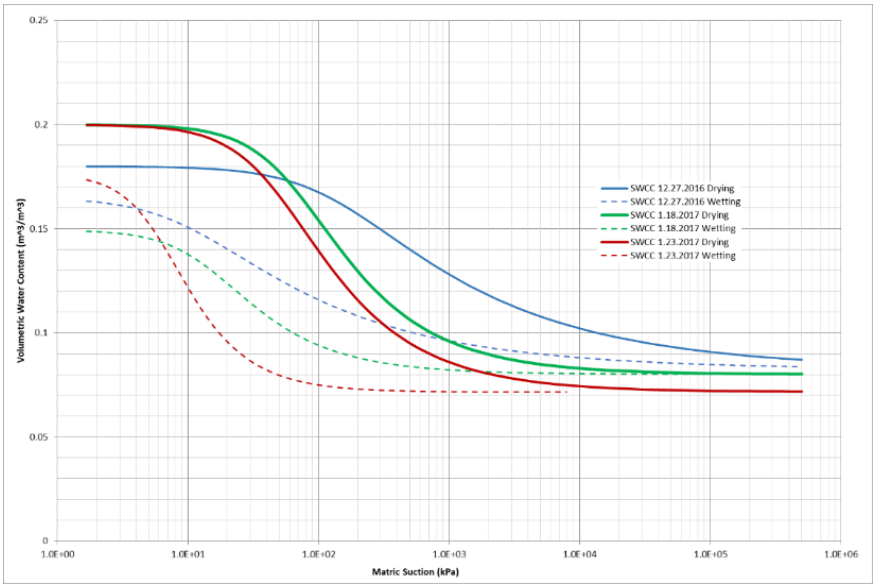

Figure 2.1 Illustration of the SWRC for the TRIM

2.3 Experimental Setup

The axis translation technique was used in this study to control the suction in the specimen. This technique involves controlling the pore air and water pressures using a high-air entry (HAE) ceramic disc. Specifically, air pressure is applied to the top of the soil specimen through a porous stone disk while water pressure is applied to the bottom of the specimen through a HAE ceramic disk. The difference between the air pressure and the water pressure is the matric suction. The bottom end cap has a fixed HAE ceramic stone which had an air-entry suction of 100 kPa, a thickness of 7.62 mm and a diameter of 42 mm and the top end cap has a fixed porous stone with the same dimensions. After preparing the specimen, the soil is enclosed within a latex membraned. Next, the confining pressure applied to the cell, provides a seal between the membrane and the specimen. One “O” ring

was placed on the top end cap and two “O” rings on the bottom to ensure a good seal on the soil specimen.

In the saturation stage, water backpressure is applied to the top and bottom end caps. The use of backpressure eliminates the possibility for air bubbles during the test giving better readings on the burettes. When applying the matric suction, the backpressure is kept constant at the bottom end cap, and the air pressure is applied from the top end cap at a value equals to the matric suction plus the backpressure.

Water movement from the specimen during: consolidation, application of matric suction and shearing stages was measured using a data acquisition software. To check the measurements, visual observation of the graduated burettes (1 ml precision) was used, this precision gave a reasonable means to check values.

The apparatus used in this testing program is a GeoTac triaxial system modified for measuring unsaturated soil properties. The system consists of two DigiFlow air pumps, a pressure panel modified for automated volume change measurements, a triaxial cell modified for volume change measurements, and a GeoJac for controlling the vertical stress. The system is manufactured by Trautwein Soil testing Equipment in Houston, Texas. All the triaxial tests were conducted in a temperature controlled room.

The double cell walls eliminate the compliance errors associated with single cell when measuring overall specimen volume changes. The triaxial cell is constructed of transparent Plexiglas material and accommodates cylindrical specimens up to 50-mm in diameter with length to diameter ratio between 2 to 2.5. The system includes differential pressure sensors mounted on the air pumps to allow for automatically recharge the pressure

controllers. The system software provides real time display and/or control of testing parameters including stresses, strains, etc.

2.4 Testing Procedures

The multistage testing methodology performed for this research involves loading-unloading a soil specimen prepared at same conditions (compaction energy and optimum water content) while applying a constant matric suction under successively higher net confining pressures. Three values of matric suction ψ of 20, 50, 95 kPa and three different net confining pressure σ_3 of 50, 100, 200 kPa were used to evaluate the shear strength for different suction and net confining pressure levels using a consolidated drained (CD) triaxial test.

After preparing the sample, all lines are flushed from air and/or water. Per the equipment setup, a minimum seating confining pressure σ_3, of 13 kPa was applied to the cell. Water was then introduced into the top and bottom endcaps to saturate the ceramic disk, soil specimen, and lines. Then, the confining pressure was increased to 70 kPa and the back pressure (manually applied from the panel to both top and bottom of the specimen at this point) was increased to 40 kPa, corresponding to a net confining stress of 30 kPa. The confining pressure and water backpressure is then increased in increments and checked until a Skempton's B-value of 0.95 was achieved. The Skempton's B value parameter is checked during the process to evaluate the saturation of the soil specimen. After completing the saturation process, the confining pressure was then increased to reach the desired initial effective confining pressure of 50 kPa in 5 kPa increments per hour. The consolidation stage is conducted for a minimum of 24 hours until no water movement is observed.

After consolidation was reached, and before applying air pressure, the top and bottom valves are closed to maintain a constant pressure in the sample. Then, the air pressure is applied from the top endcap at a value equals to the backpressure (zero matric suction). At the same time, air is applied to flush the top endcap and drainage lines connected to the top of the specimen. In each test, for example; for 20 kPa matric suction test, the air pressure was increased by 20 kPa difference between the top (air pressure) and bottom (water pressure). The same procedure was used for the other two matric suction values (50, 95 kPa). The water outflow (pore volume) from the specimen was recorded during the application of the matric suction using both, the data acquisition software and burettes and sufficient time was permitted to reach equilibrium (or no water outflow).

After equilibrium is reached for the matric suction stage, the CD triaxial test is started. For the saturated and unsaturated tests, a constant shearing rate of 0.28 and 0.10 mm/hour was used, respectively. These values where selected using the equations presented by Ho and Fredlund (1982) for strain rates for unsaturated soil shear strength testing. The pore water pressure were monitored during shearing to confirm that the shear rates were low enough for pore water pressure to dissipate. At each step, drainage of both air and water was permitted. The shear stress was evaluated at the peak principal stress ratio σ_1/σ_3.

2.5 Results and Discussion

The shear strength of single stage and multistage CD triaxial tests for saturated and unsaturated soil specimens has been analyzed at an introduced matric suction of 20, 50, 95 kPa and net confining pressures of 50, 100, 200 kPa. The purpose of the analysis is to

compare the multistage triaxial test to conventional single stage triaxial test as well as unsaturated to saturated conditions on a highly compacted silty sand material. The single stage tests have been denoted in the legend as solid lines, whereas the multistage tests have been represented by dotted lines. The net confining pressure "σ_{3n}" equals to $(\sigma_3 - u_a)$ and is labeled on each particular test. The matric suction $(\psi = u_a - u_w)$ is presented as constant during the tests and is labeled in the top left of the plot.

2.5.1 Multi-stage Triaxial Testing

The principal stress difference is plotted as a function of axial strain in Figure 2.2 for the CD multistage shear tests for saturated and unsaturated specimens subjected to different, matric suction (ms=20, 50, 95 kPa) and net confining pressure ($\sigma_3 - u_a$ =50, 100, 200 kPa).

As observed in Figure 2.2, when increasing both the matric suction and the confining pressure, the deviatoric stress and hence the shear strength increases. In general, the behavior was as expected since increasing the matric suction results in an increasing in the effective stress. The saturated tests peak strengths were lower than the unsaturated tests.

Also, as observed in Table 1, in the saturated test the axial strain corresponding to maximum stress ratio (MSR) increased as the net confining pressure is increased. As observed, the axial strain from the saturated at the corresponding MSR is 0.8% at the 50 kPa net confining while for the unsaturated test at 20 kPa matric suction, a 2.03% of axial strain at the MSR was obtained.

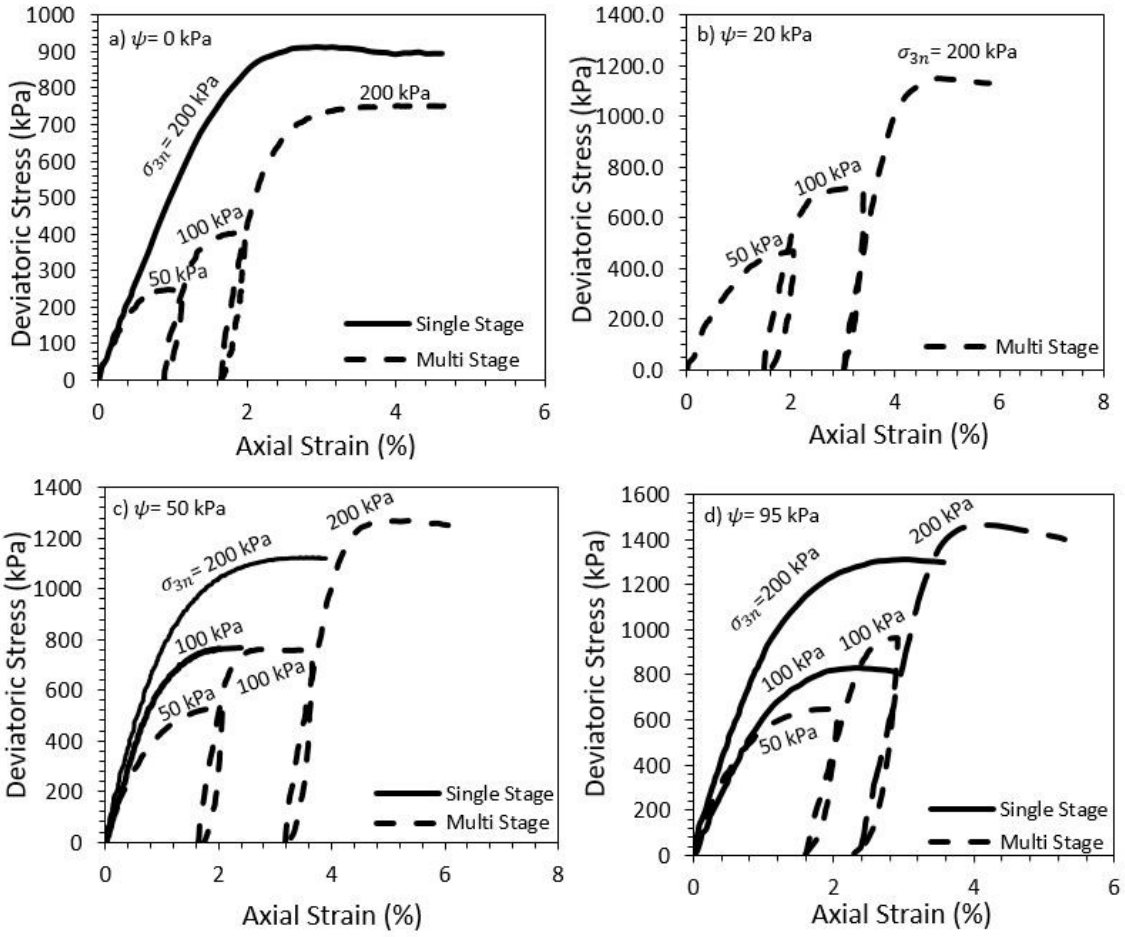

Figure 2.2 Principal stress difference versus cumulative axial strain of (a) saturated, (b) ms= 20 kPa, (c) ms= 50 kPa and (d) ms = 95 kPa from single stage and multistage tests

On the other hand, for the unsaturated test at a constant matric suction, as the net confining increases from 50 to 100 kPa the axial strain decreases. In general, for most of the matric suction tests at the next two increments of net confining pressure the axial strains were decreased. It seems that the sample undergoes into a more plastic behavior after the first stage which results in reducing the axial strain at which the peak strength occurs in the following stage.

Table 2.1 Multistage tests Results at the Maximum Stress Ratio (MSR)

Type of Test	Matric Suction (kPa)	Net Confining Stress (kPa)	Axial Strain at MSR (%)	Deviatoric Stress at MSR (kPa)
Multi Stage	0	50	0.80	244.69
		100	1.08	504.00
		200	2.31	749.16
Multi Stage	20	50	2.03	470.42
		100	1.58	818.76
		200	1.79	1348.97
Multi Stage	50	50	2.06	531.74
		100	1.28	760.48
		200	2.20	1268.58
Multi Stage	95	50	1.95	650.28
		100	1.27	965.61
		200	1.84	1465.92
Single	0	200	2.94	914.59
Single	50	100	2.40	764.70
Single	50	200	3.55	1124.81
Single	95	100	2.33	828.59
Single	95	200	3.04	1313.00

Figure 2.3 shows the shear stress for saturated and unsaturated conditions at different matric suctions and different net confining pressures. The slope of each of these lines provides the effect of the matric suction on the increase of the shear stress; tan ϕ^b. As observed, ϕ^b equals to ϕ' at saturation (ms = 0 kPa). ϕ^b is not constant and decreases at higher matric suction. These results are consistent with the finding presented by Leong et al 2013, were there results showed that ϕ^b is not constant, but decreases as matric suction is increased. In other words, as the ϕ^b increases the effect in shear strength of the material in the unsaturated zone will be increased. At certain value of matric suction, the shear strength of the material will not increase, and will remain constant or decrease.

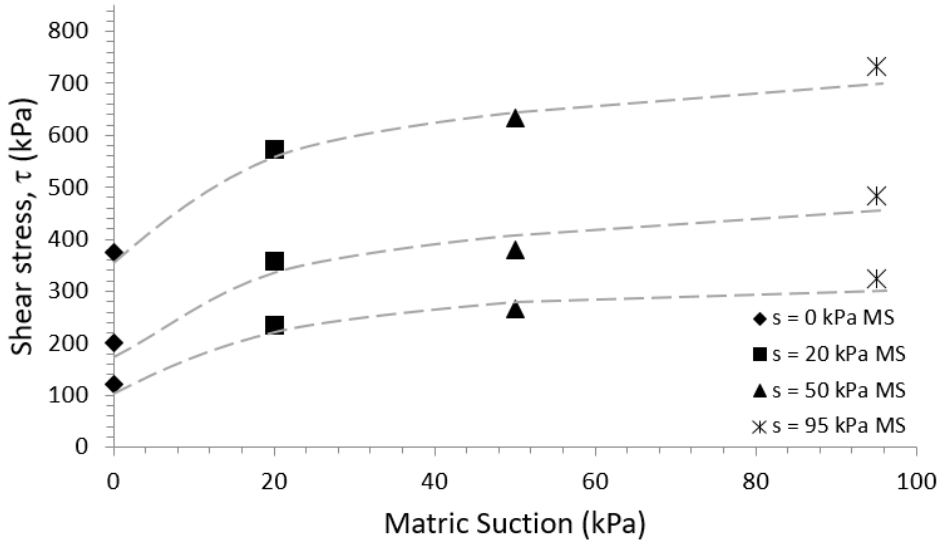

Figure 2.3 Shear Stress at different matric suction to determine ϕ^b

2.5.2 Single Stage Triaxial Testing

The single stage triaxial tests were conducted at a net confining pressure of 200 kPa at three different matric suctions *ms* = 0, 50, 95 kPa, and at a net confining pressure of 100 kPa at two matric suctions *ms* = 50, 95 kPa. The first stage of the multistage triaxial test at a net confining pressure of 50 kPa were also considered in this discussion as single stage tests. The results of the deviatoric stress versus axial strain for single stage are shown in Figure 2.4, as observed the shear strength of the soil increased with the increase in matric suction. As observed on the Figure 2.4a, the axial strain for the saturated test at 200 kPa net confining is reached before 3% compared to the partially saturated soils where the peak axial strain reaches more than 3%. Also, on Figure 2.4b, the deviatoric stress versus axial strain for 50 kPa net confining pressure is presented. As observed, the stress increases with an increment in matric suction. The peak axial strain also increases as the matric suction

increases. For 50 kPa net confining pressure, the axial strain of the saturated test at the maximum stress ratio was around 1% in compared to the partially saturated tests were the maximum stress ratio was reached at 2%. The change in axial strain is substantial when using a lower net confining pressure (50 kPa) in compared to a higher net confining pressure (200 kPa) where there is some minimum difference.

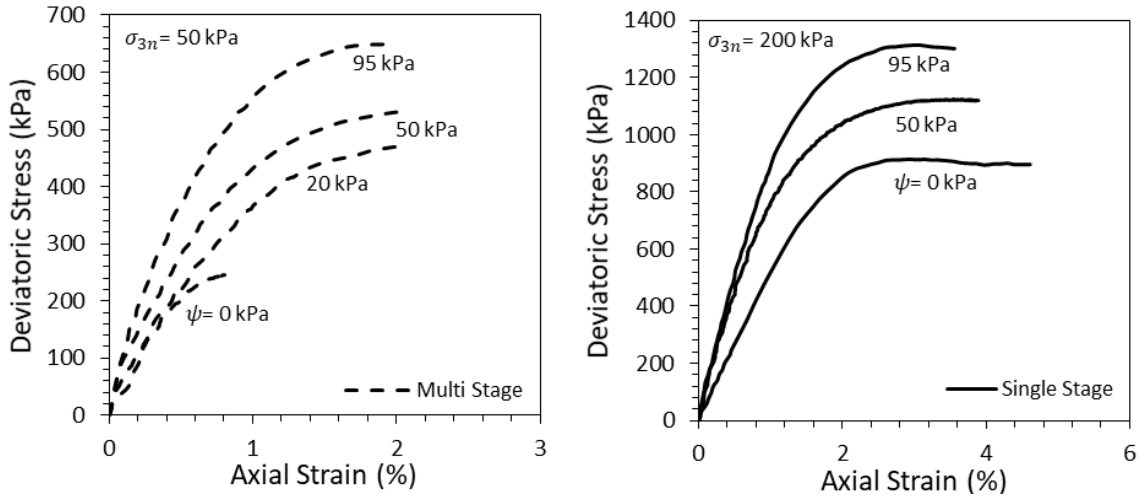

Figure 2.4 Stress-strain curves of single stage triaxial tests for saturated and unsaturated specimens

Also, Figure 2.4 shows a variation in the modulus of elasticity of the material, as the matric suction increases the slope of the stress versus strain curve, i.e. the modulus of elasticity increases. This is consistent with the observations of other investigators in the literature (Fredlund and Rahardjo, 1993; Costa et al., 2003; Inci et al., 2003; Lu and Likos, 2006; Yang et al., 2005, 2008; Oh et al., 2009; Vanapalli and Oh, 2010).

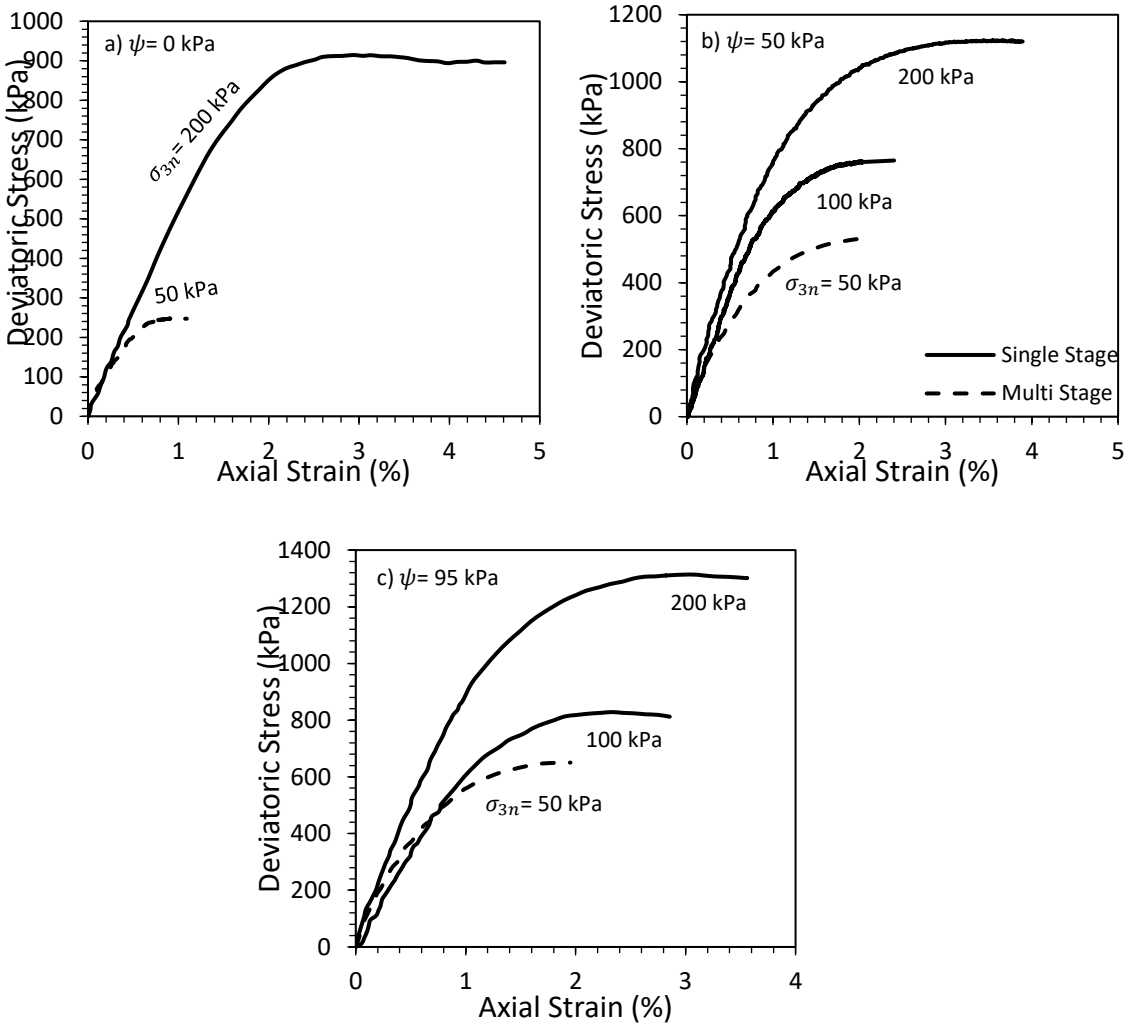

Figure 2.5 Stress-strain curves of single stage triaxial tests for: (a) 0 kPa, (b) 50 kPa and (c) 95 kPa matric suction in respect to the net confining pressures of 50, 100, 200 kPa.

For constant 50 kPa matric suction, the higher net confining pressure results in higher shear stress, it increases from 532 to 765 to 1225 kPa, when net confining pressure increases from 50 to 100 and 200 kPa, respectively. The corresponding axial strain also increases from 2.06% to 2.40% to 3.55%. For constant 95 kPa matric suction, the higher net confining pressure results in higher shear stress, it increases from 650 to 834 to 1313

kPa, when net confining pressure increases from 50 to 100 and 200 kPa, respectively. The corresponding axial strain also increases from 1.95% to 2.33% to 3.04%.

2.5.3 Single versus Multistage Triaxial Testing

Figure 2.2 shows the comparison between the deviator stress response obtained from single-stage and multistage triaxial tests at a saturated condition and at a matric suctions of 50 and 95 kPa. The multistage test were performed at confining pressures of 50, 100, 200 kPa while the single stage tests were performed at a net confining pressures of 100 and 200 kPa.

It is evident that for 50 and 95 kPa matric suction levels, the deviatoric responses obtained from multistage test at 200 kPa net confinement are slightly less compared to the results from single stage. On the other hand, for the single stage test of 50 kPa matric suction at 100 kPa net confinement the deviatoric response is similar to the multistage at the same net confining pressure and matric suction. Also, for the saturated specimen the 200 kPa net confinement single-stage was about 200 kPa higher than the third stage of the multistage test at 200 kPa net confinement. It seems that at higher confining pressure the single stage peak is below the multistage, but for lower confining pressures the peak is higher or at the same response. For saturated tests the peaks behave the opposite to the unsaturated soils, where the peak value is higher than multistage test.

Figure 2.6 shows the volume change comparison between single stage and multistage for unsaturated soils. The plot shows the results from multistage at 95 kPa matric suction with variations in the net confining pressures (50, 100, 200 kPa). Also, the single

stage volume change results from 100 kPa and 200 kPa for the same matric suction (95 kPa) are shown.

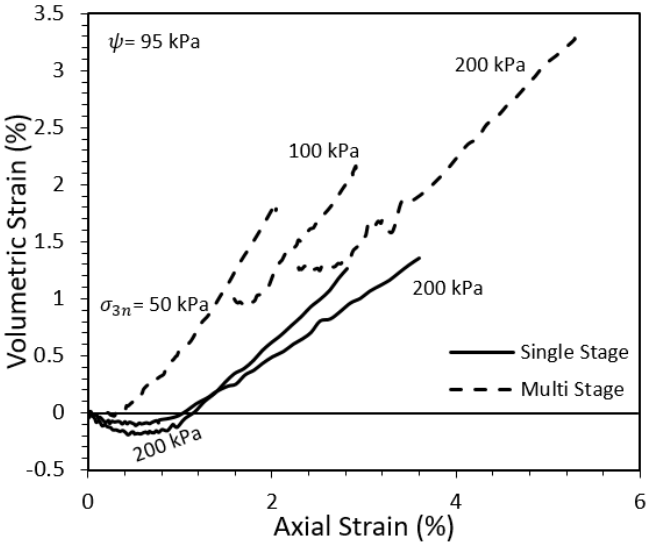

Figure 2.6 Volumetric strain for multistage and single stage test

Figure 2.7 shows the peak state lines (PSL) obtained from the single and multistage triaxial tests in the p'-q plots. The MIT formula was used to generate the p'-q plots. The slope of the saturated PSL, M is 0.67 corresponding to an "a" of 0 kPa. The shear strength parameters obtained from the saturated test are the following: c' = 0.0 kPa and a ϕ' = 41.3°.

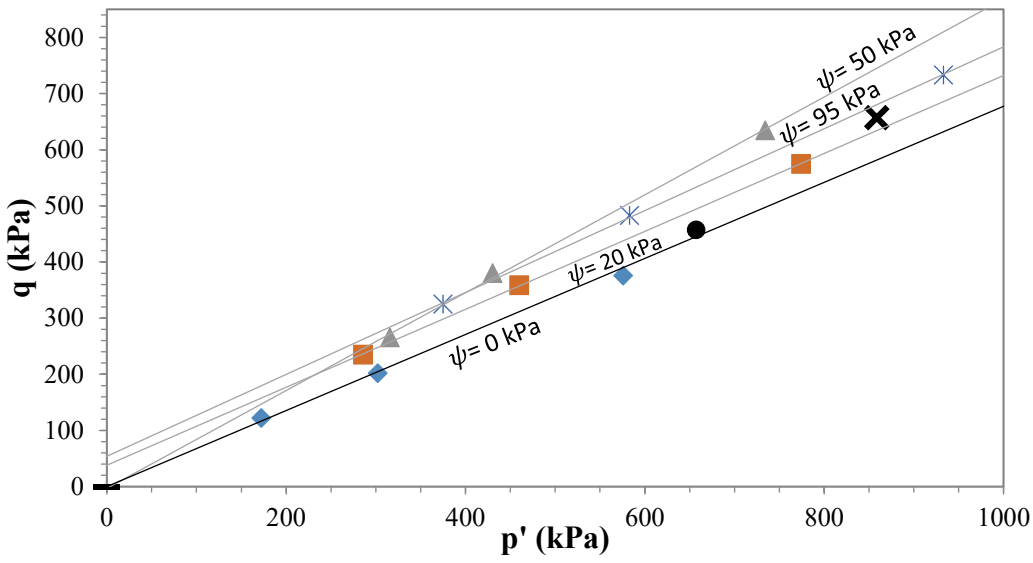

Figure 2.7 PSLs for low to medium suction states

In general, the slopes of the PSL for low to medium suction states are similar. The only test that does not follow a constant slope is the suction equal to 50 kPa. On the other hand, the 20 and 95 kPa suctions seems to have a similar slope as the saturated test. Also, an increment parallel to the saturated line is observed as the matric suction is increased, that can be possible due to the apparent cohesion in unsaturated specimens.

CHAPTER III

CASE STUDY: INTEGRATING FIELD MONITORING AND NUMERICAL MODELING TO EVALUATE PERFORMANCE OF A LEVEE UNDER CLIMATIC AND TIDAL VARIATIONS

3.1 Introduction and Background

Assessing the performance and stability of earthen structures during their service life warrants an improved understanding of the behavior of variably saturated soils under transient seepage conditions. The need is more pronounced considering recent climatic trends, which have led to more frequent and severe extreme events. Climate change has caused considerable changes in intensity, frequency, and duration of extreme precipitation events in several parts of the world (IPCC, 2013; USGCRP, 2009). In the United States, an increase of 20% in the amount of heavy precipitation is reported from 1958 to 2007 (USGCRP, 2009). In several regions, heavier rainfalls occur over shorter periods of time, posing a real flash flood threat to the levees in that region due to the huge quantity of runoff produced in a short time. Ragno et al. (2018) employed a non-stationary model and showed that major cities in the United States might experience extreme precipitation events up to 20% more intense and twice as frequent compared to historical records. Aforementioned changes in the statistics of extreme precipitations and flood probability can affect the stability of earthen structures through changes in degree of saturation (e.g., Vahedifard et al., 2016a; Robinson et al., 2017; Jasim et al., 2017; Vahedifard 2017a,b).

Several short-duration and extreme hydraulic loadings (e.g., flooding, extreme precipitations, rapid drawdown) can impose earthen slopes and embankments to time-dependent seepage conditions. Numerical modeling of an earthen structure subjected to such scenarios warrants performing transient seepage analysis under variably saturated conditions. Earlier attempts in this area primarily involve transient saturated seepage analyses of rapid drawdown in earthen dams (e.g., Freeze, 1971; Stark et al., 1987). Improved understating of the theory along with continuous advances in numeral modeling of flow in porous media have extended the realm of transient seepage analyses to unsaturated soils. Some example applications include modeling rainfall-triggered landslides in natural slopes (e.g., Godt et al., 2012; Leshchinsky et al., 2015), analysis of saturated-unsaturated rapid drawdown in earthen dams (e.g., Stark et al., 2016), and simulation of the hydro-mechanical behavior of unsaturated earthen structures under extreme precipitation and flood events (e.g., Jasim et al., 2016; Vahedifard et al., 2018).

A group of previous transient seepage analyses are performed through solving the governing equation of unsaturated flow (i.e., Richards' equation) using an analytical solution or numerical method (e.g., finite element, finite difference) and then incorporating the seepage analysis results into a limit equilibrium or limit analysis of the earthen structure (e.g., Godt et al., 2012; Stark et al. 2017). Alternatively, coupled hydro-mechanical simulations are also performed using more advanced numerical models to account for the two-way interaction between solids and fluid (e.g., Jasim et al., 2016; Vahedifard et al., 2017b). The former group requires fewer input parameters and computational resources but is still shown to provide reasonable results for several applications. The latter group

involves more rigorous molding efforts, but with appropriate input parameters and model setting, can lead to more accurate results. This observation becomes particularly important for models where the soil compressibility is considerable and/or the change in total stress is significant.

Considerable research advances have been made in various aspects of variably saturated transient seepage. Some of these research findings have been translated to the state of the practice. For example, several commercial software programs have been developed that are designated to facilitate variably saturated transient seepage analyses. However, the geotechnical engineering community has been relatively hesitant to fully embrace transient seepage analysis in practice. Difficulty to assign appropriate input parameters and boundary conditions, and lack of practical guidelines are among the main factors that have hindered the widespread application of numerical modeling of transient seepage in the state of the practice. Further, lack of full-scale validation of the results and poor connection to field monitoring data undermine the validity and accuracy of such numerical analyses to practicing engineers. Best practices need new guidelines to provide instructions for where and when transient seepage can be applied in a useful and correct manner due to the uncertainty and inexperience of practicing engineers. For instance, the main guidance documents used for seepage analysis of levees and dams for the U.S. Army Corps of Engineers (USACE) projects are Engineer Manual (EM) 1110-2-1901 (USACE, 1993) and EM 1110-2-1913 (USACE, 2000). Although these EMs acknowledge the existence of transient seepage conditions, they do not provide any guidance regarding the use of transient analyses for partially saturated soils in engineering practice.

This case study paper aims to demonstrate how to effectively employ field-monitoring data to improve the numerical analysis of a levee under climatic and tidal variations. The case study includes a silty sand setback levee located near Seattle, Washington (WA). The study area, levee section, and instrumentation plan are discussed. The data collected from the sensors are used to monitor suction stress and effective stress versus time. A finite element model of transient seepage under saturated-unsaturated conditions is then developed and calibrated to reasonably match the measured pore-water pressures and the piezometric surface. The application of the numerical model is illustrated by modeling the seepage and stability of the levee during a 100-year flood.

3.2 Study Site: Qwuloolt Levee

3.2.1 Study Area

Approximately 162 hectares (400 acres) of estuarine restored land in WA form one of the largest ecosystem restoration projects in the United States. The project site is located about 64 kilometers (40 miles) north of Seattle, WA. As part of this project, a 1,219-meter (4,000 feet) long setback levee, named Qwuloolt levee, was constructed using silty sand in 2014 to protect an industrial area behind it, while allowing for the site to be inundated with the Puget Sound water. Figure 3.1 shows the study area, located in the city of Marysville, Snohomish County, WA with the Puget Sound and the Central Cascade mountain range bounding it to the east and west, respectively. The project borders include the city's sewage treatment plant to the west, an industrial park to the northwest, residential neighborhoods along 61st Street NE, and Sunnyside Boulevard to the north and east, respectively.

Figure 3.1 Map of Study Area and Levee Section (source: Google Maps).

In general, the regional ground surface elevation gradually slopes from 48 meters (160 feet) in the north to 1.5 meters (5 feet) in the southern parts of Marysville. The study area has an average ground surface elevation of about zero. The climate is defined as temperate/mesothermal, with an average rainfall of 1043 mm (41 inches). The topsoil extends down to 1 meter (3.3 feet), is classified as a hydric Puget silt loam (Anderson, 1947), and is representative of the levee and the surrounding area. The initial soil horizon extends to 152 mm (6 inches) depth and is a brownish gray to gray smooth friable silt loam with relatively high organic matter content (Anderson, 1947). The subsoil has a noticeable laminated structure and is a light gray silt loam to a depth of 508 mm (20 inches). Between 508 mm to 1016 mm (20 to 40 inches), the soil is a brownish-gray silty clay loam with a layered structure. Stratified layers of yellowish-brown colored sandy loams and fine sands with a greenish-gray tint underlie the silty clay loam horizon (Anderson, 1947).

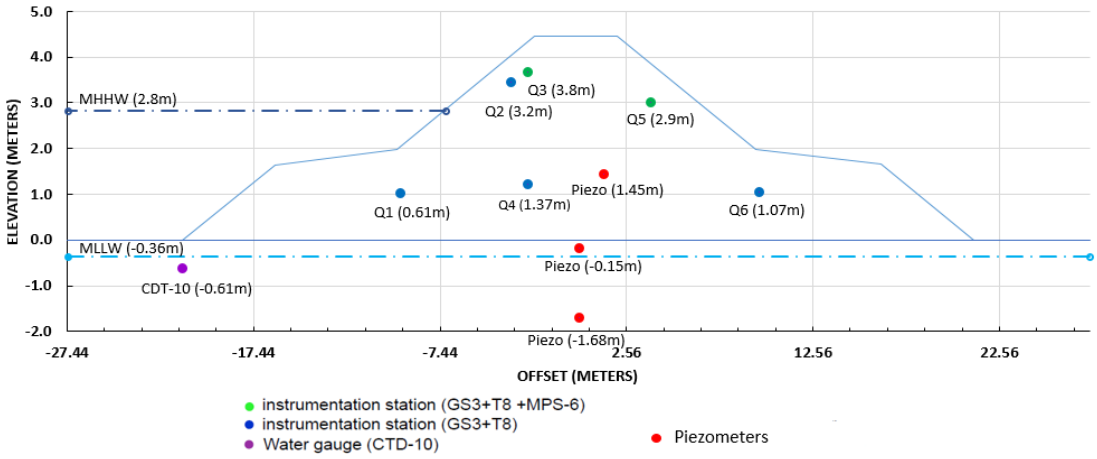

Figure 3.2 Instrumented Section of Levee (station 36+10).

3.2.2 Field Instrumentation Plan

Figure 3.2 depicts a cross section of the levee (station 36+10), which is instrumented with different sensors made by METER Group, Inc. for field monitoring purposes. As shown in Figure 3.2, the levee is instrumented to measure water content, electrical conductivity, suction, temperature, and tidal water level. Figure 3.3 provides further details about the location and depth of the sensors.

Two tensiometer types are used in this study: T8 and MPS-6. The T8 tensiometer, shown in Figure 3.4b, consists of a combined sensor for matric potential and temperature for long-term monitoring purposes. This type of tensiometers has a working range from -85 kPa to 100 kPa of water pressure with a soil water tension accuracy of ± 0.5 kPa (METER Group, 2018). A porous ceramic cup filled with water is in direct contact with the soil water. The soil water tension is measured by a pressure transducer. The MPS-6 tensiometer, shown in Figure 3.4c, has measurement range from -100,000 kPa (air dry) to -9 kPa with an accuracy of ± (10%+2kPa) (METER Group, 2018). The GS3 moisture

sensor, shown in Figure 3.4d, measures the water content, electrical conductivity, and temperature of soil. The GS3 sensor uses an electromagnetic field to measure the dielectric permittivity of the surrounding medium, which is converted to water content by a calibration equation. The CDT-10 sensor measures the tidal water level, electrical conductivity, and temperature in both ground water and surface water. The water depth resolution is about 2 mm, and accuracy is ±0.05% of full scale at 20°C (METER Group, 2018). In addition, a weather station at the site is used to obtain the precipitation in the study area as well as other weather parameters like temperature, humidity, and wind speed. Precipitation data is used to evaluate the changes in pore pressure and volumetric water content due to rainfall events.

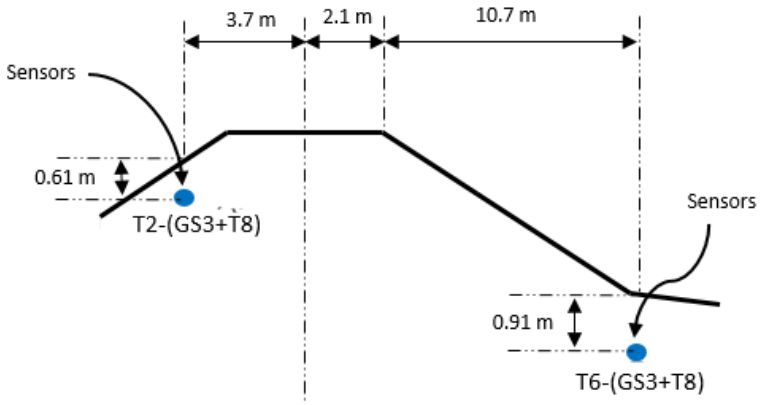

Figure 3.3 Location of Sensors within the Levee Embankment.

The construction of the levee started in 2012 and ended in 2014. The instruments were installed during the week of August 10-17, 2015. To deploy the instruments at the designated depths, boreholes were drilled using hand auguring (Figure 3.5). Sensors were installed by placing them at the desired depth and then were surrounded by compacted soil.

A PVC pipe was used to keep the borehole stable. After installing the sensors, the boreholes were sealed with bentonite slurry and PVC caps. Soil samples were collected at different intervals from all the holes.

During construction of the levee, two piezometers were installed in the levee foundation and have been monitored ever since then. After about one year from the sensors installation (September 7, 2016), a third piezometer (Piezo4.75) was installed as an open well to measure the water elevation (i.e., phreatic surface) within the embankment (Figure 3.2).

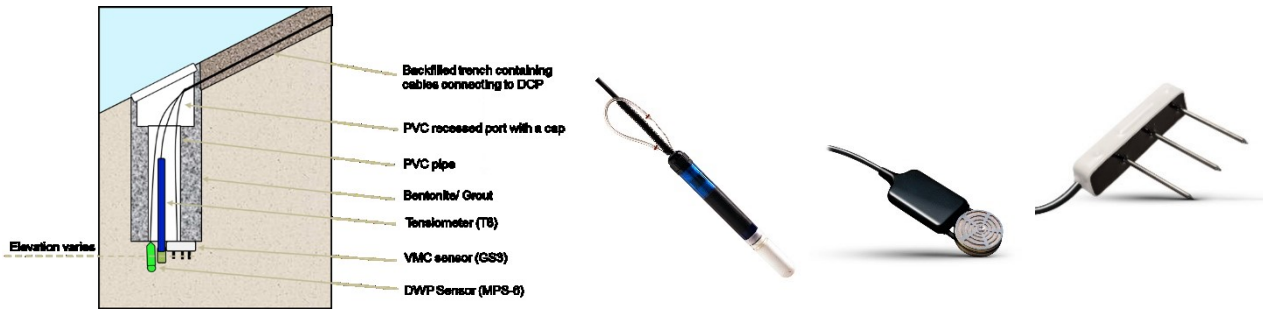

(a) (b) (c) (d)

Figure 3.4 Sensors Installed at Each Section: (a) Sensors diagram, (b) T8-tensiometer, (c) MPS6-tensiometer, and (d) GS3-moisture sensor.

Figure 3.5 Hand Drilling of Instrumentation Holes.

The weather sensors collect data every 6 hours. The sensors and the data logger are powered by a solar panel. The soil sensors are connected to underground cables to protect them from any damage. The soil data loggers have their own solar-charged batteries, which help to maintain the power on the system. The water gauge CTD-10 is placed in a trench close to the levee toe on the water side. The water gauge was placed in a perforated 10-cm PVC pipe wrapped in a protective textile sleeve below the low water table. The trench was then backfilled with filter rock. METER's Em50 modem is used to collect and transmit the data using METER's software.

3.2.3 Instrumentation Readings

Figures 3.6 to 3.11 show instrumentation readings from September 7, 2016 to November 27, 2017. Figure 3.6 shows the pore pressure at stations Q2, Q5, and Q6. Tidal and piezometer readings are converted to total head for comparison. The water table on the downstream side is typically close to the ground surface most of the time. It is anticipated that the soil suction at location Q6 is not high due to the presence of the phreatic surface, which elevates the moisture content and pore pressures due to the proximity of the water table. At location Q2, suction is expected to be higher than Q5 and Q6, because Q2 has a higher elevation relative to the phreatic surface. The initial two months are considered the end of a drought period. Then, from October 2016 to June 2017, no substantial changes in suction were observed due to the rainy season (winter season).

As evident in Figure 3.6, one dry period is captured by the tensiometers from September 7 to October 19, 2016. For this period, the Q2 and Q6 pressure sensors show an increment in pore-water pressure in response to this change in moisture content (Figure

3.7) during October 12, 2016, as the same time. For the Q5 pressure sensor, the change is noticed in October 19, 2016 on both pore pressure and volumetric water content (Figure 3.7). After mid-October 2016 to June 2017, the pressure sensors were reading constant values while the changes in volumetric water content were minor.

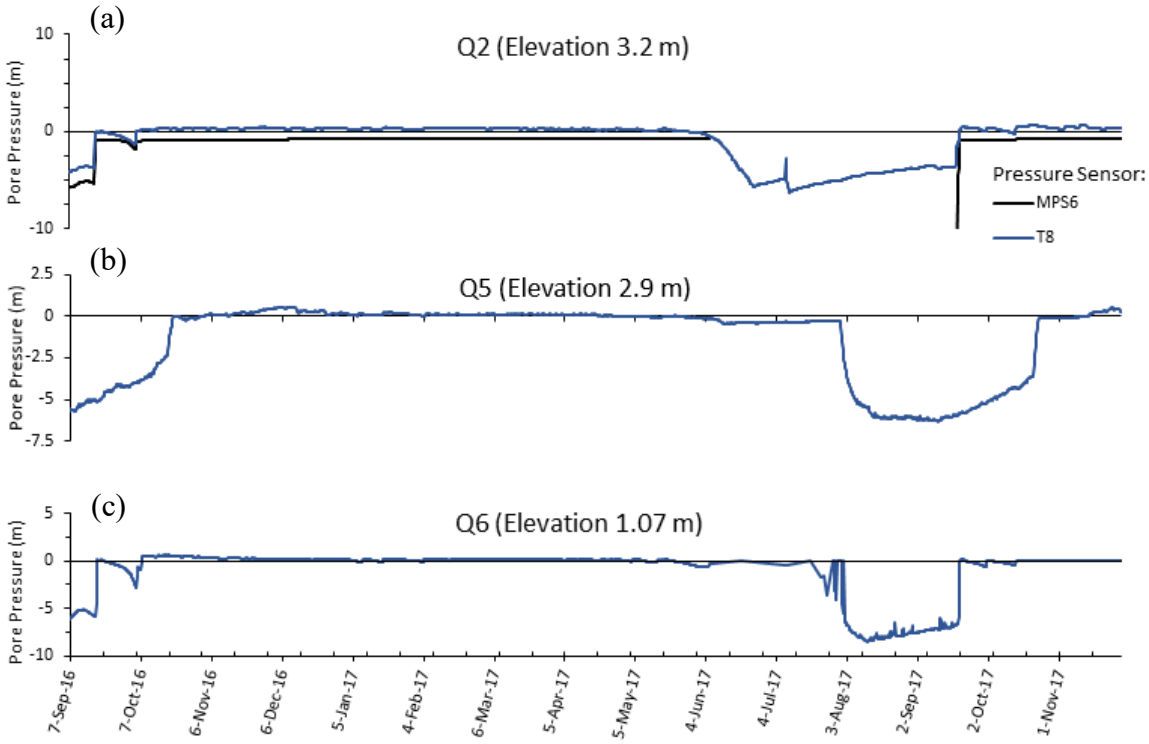

Figure 3.6 Pore Water Pressure versus Time for: (a) Q2, (b) Q5, and (c) Q6.

Station Q2 has two different types of sensors at the same elevation: MPS-6 and T8. In general, the readings from these two sensors follow the same pattern, but MPS-6 is reading values higher in negative pore pressure. It is observed that a combination of changes in the water tides and precipitation does not directly influence the pore pressures/matric suction or the volumetric water content.

During the monitoring period, two dry events were observed, the first is from September 2016 to October 2016, where a drop is observed in the matric suction for Q2, Q5, and Q6. The second dry event is from June 2017 to September 2017 were matric suction has drop for all stations. It is confirmed that minor to zero precipitation was observed during both periods. The time lag in the matric suction was observed for the monitored stations to be two to three weeks.

Figure 3.7 shows the volumetric water content at stations Q2, Q5, and Q6 versus time. For station Q2 and Q6, the GS3 sensors recorded a change in volumetric water content during the period between September 7, 2016 and November 27, 2017, when a precipitation event occurred having a change in volumetric water content from 0.22 to 0.38 (m^3/m^3). The Q5 water content remain constant during that period until October 19, 2016, where a change is noticed from 0.21 to 0.38 (m^3/m^3). All volumetric water content stations experienced a drop during the drought period of June 2017 to September 2017.

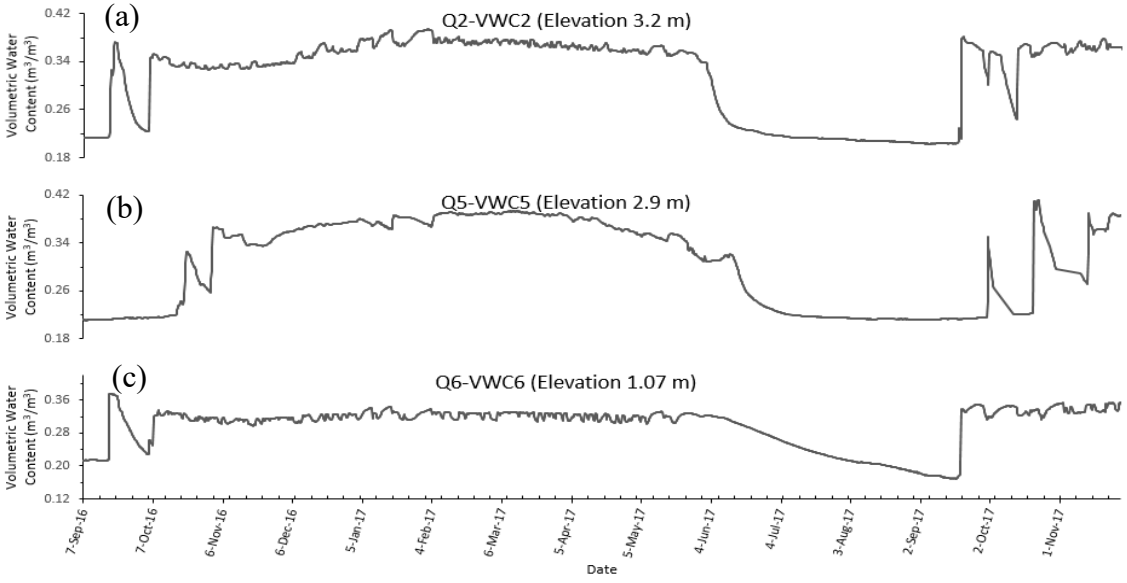

Figure 3.7 Volumetric Water Content versus time for: (a) Q2, (b) Q5, and (c) Q6.

For all stations, the GS3 sensor recorded a nearly constant in volumetric water content during November and December 2016 months. The constant pattern confirms that station Q6 is close to the water elevation, which means that the soil is close to the saturated condition at that moment. For the period of study, the saturated volumetric content is the highest value observed by the sensors (0.39 m^3/m^3), and the residual volumetric water content observed is 0.20 m^3/m^3.

Figure 3.8 shows the temperature, relative humidity, and piezometer data for the levee during the period of September 2016 to November 2017. As observed in Figure 3.8a, the temperature overall fluctuates, decreases, and increases in the time period. The relative humidity in Figure 3.8b fluctuates substantially during the day but goes back to the same baseline. The Piezo el. -0.152 m and Piezo el. -1.68 m do not change substantially with the changes of the tide and precipitation. These events seem to be disconnected from the embankment due to the silt layer. The Piezo 4.75 (Piezo el. 1.44 m) seems to be affected substantially after December 7, 2016.

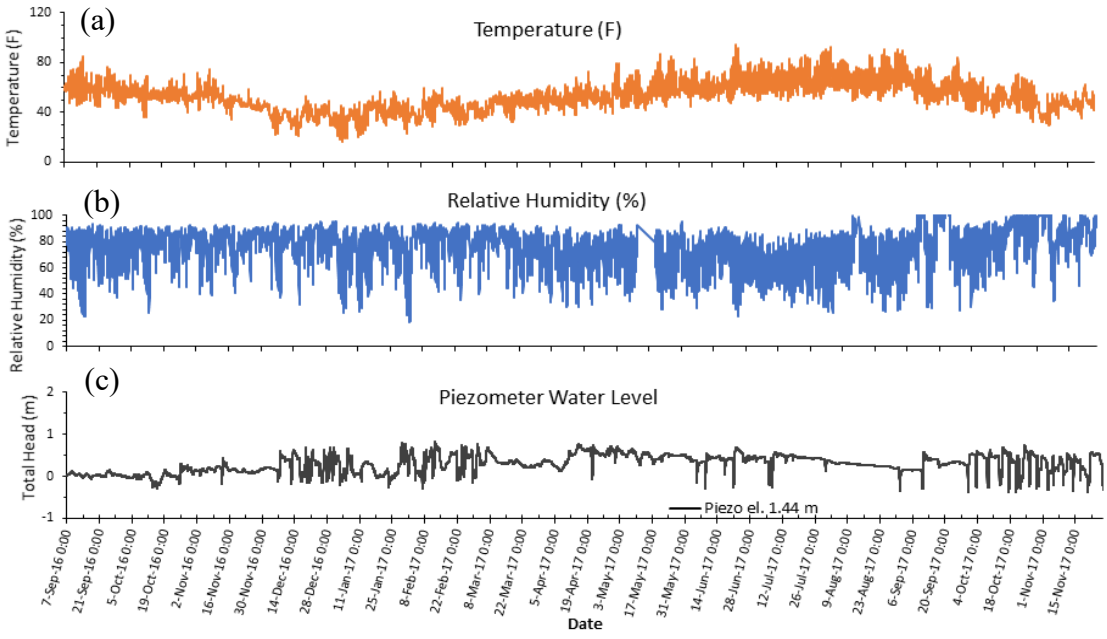

Figure 3.8 Temperature, Relative Humidity and Piezometer Water Level for the Period of Study.

As shown in Figure 3.9, CDT-10 data show that the tidal elevations varied during the day but follow a constant pattern during the 15-month period (from September 2016 to November 2017) with a high tide ranging from 2.5 to 2-m, and low tide was approximately 1 m.

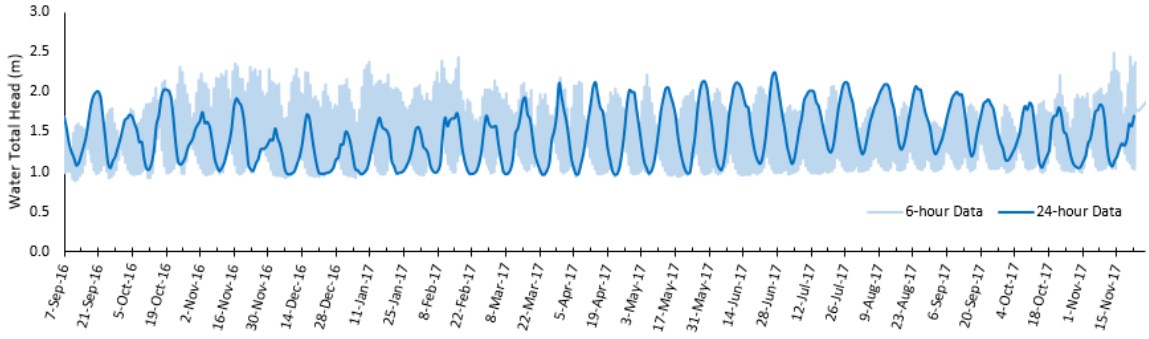

Figure 3.9 Tidal Hydrograph with 6-hr and 24-hr Data for Qwuloolt Levee

Figure 3.10 depicts the precipitation at of the site. As shown in Figure 3.10, the precipitation data shows that the rainfall events started during the period of September 2016 to November 2017; no rainfall was recorded for the rest of the period. Peak recorded precipitation ranged from 7 mm to 4 mm in 6 hours.

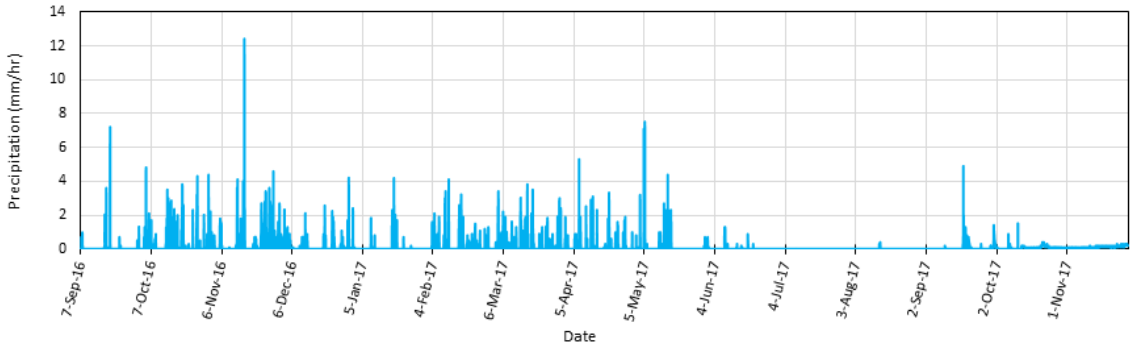

Figure 3.10 Precipitation Data for the Levee Site

Solar radiation, defined as the radiant energy emitted by the sun (measured in Watts/m^2), is one of the climatic parameters required by SEEP/W 2018 to complete the land-climate interaction boundary condition. The installed instruments at the site do not record solar radiation. The data used in this study was obtained from a publicly available database operated by Washington State University (WSU) from the Langley weather station, located in Whidbey Island about 15 miles away from the site.

As shown in Figure 3.11, the solar radiation was also considered in the Climate Boundary Condition (CBC), and the modeling period started in September 7, 2016. As observed, the radiation varied from 1000 W/m^2 to 300 W/m^2 on the higher range and a lower value of 100 W/m^2. The ASCE Standardized Reference for Evapotranspiration (Allen et al. 2005) recommends an albedo reflection coefficient value of 0.23 to calculate the net radiation from the measured short-wave radiation presented in Figure 3.11.

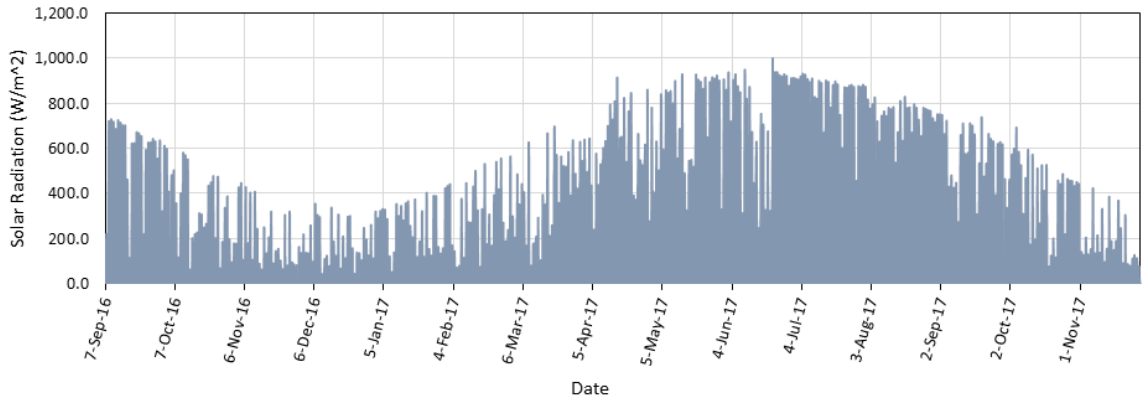

Figure 3.11 Solar Radiation

One can calculate the net radiation using the net solar or net short-wave radiation R_{ns}, resulting from the balance between the incoming and reflected solar radiation given by:

$$R_{ns} = R_s - \alpha R_s = (1 - \alpha)R_s \quad [3.1]$$

where:

R_{ns}= net solar or short-wave radiation.

α = albedo or canopy reflection coefficient, is fixed at 0.23 for the standardized short and tall reference surfaces [dimensionless], and

R_s= incoming solar radiation.

Allen et al. (1994) concluded that albedo varies somewhat with time of day, time of season, and latitude due to change in sun angle. However, because the solar intensity is less during these periods, the error introduced in fixing albedo at 0.23 is relatively small (Allen et al. 1994).

3.2.4 Laboratory Testing

Representative soil samples were collected from different locations of the levee's embankment and foundation and were shipped to the U.S Army Engineer Research and Development Center (ERDC) in Vicksburg, MS, for testing. Table 3.1 presents a summary of index properties of five soil samples retrieved from the two locations of interest within the levee body: Q2 and Q6. The soil is classified as silty sand (SM) as per the Unified Soil Classification System (USCS).

Table 3.1 Index properties of soil samples retrieved.

Property	T2	T3	T4	T5	T6
Passing #4 (%)	87.5	73.5	59.9	80.2	69
Passing #200 (%)	24.7	20.7	15.7	21.8	17.6
Specific gravity	2.73	--	--	--	2.76
USCS	Silty Sand (SM)	Silty Sand (SM) with Gravel	Silty Sand (SM) with Gravel	Silty Sand (SM) with Gravel	Silty Sand (SM) with Gravel

The soil water characteristic curve (SWCC) of the silty sand material was measured by running a multiple test using the Transient water Release and Imbibition Method (TRIM). Wayllace and Lu (2012) presented this methodology to provide a fast, accurate, and simple testing tool for obtaining the SWCC for various soil types under wetting and drying states. The TRIM method uses an inverse modeling technique to develop the full curve from two matric suction pressures (10 kPa and 290 kPa for this study) that are exposed to the soil.

The SWCCs shown in Figure 3.12 represent drying and wetting curves for silty sand samples retrieved from the same depth where the instruments were installed. As part

of running the TRIM test, a saturated hydraulic conductivity of $3.9e^{-05}$ cm/s was determined and used in obtaining the SWCC using the van Genuchten (1980) SWCC model. From the TRIM results, an average van Genuchten's *a* of 64 kPa and *n* of 1.6 were obtained. An average hydraulic conductivity of $3x10^{\wedge -5}$ cm/s was also obtained and used in this study.

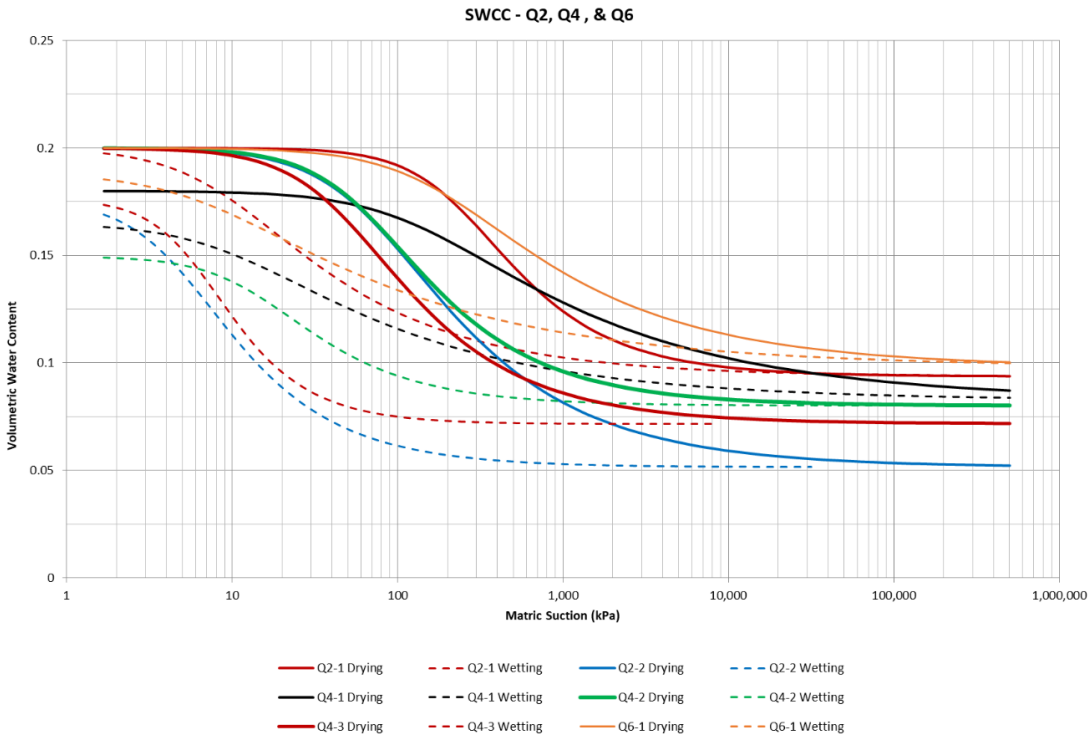

Figure 3.12 SWCCs of the Tested Soils under Drying and Wetting Paths

3.3 Monitoring Suction Stress and Effective Stress Using Field Data

This section demonstrates how one can employ in situ data consisting of pore-water pressures and water content to compute effective stress versus time. Effective stress is a critical parameter that dominates the shear strength and, subsequently, the stability of earthen structures (e.g., Lu and Likos 2004; Vahedifard et al. 2016b). Pioneered by Bishop (1959), several researchers have tried to properly characterize effective stress of

unsaturated soils. In this study, we employ the suction stress-based effective stress representation, along with the measured field data, to directly obtain suction stress and effective stress time series within the unsaturated zone of the levee body under seasonal and tidal changes.

Lu and Likos (2004) extended Bishop's expression for the effective stress of unsaturated soils by adopting the suction stress concept. The unified effective stress for both saturated and unsaturated soil conditions can be shown as (Lu and Likos 2004):

$$\sigma' = (\sigma - u_a) - \sigma^s \quad [3.2]$$

where $\sigma'$is the effective stress, σ is the total stress, $u_a$is the pore-air pressure, and $\sigma^s$is the suction stress. Suction stress for unsaturated soils can be determined by (Lu et al. 2010):

$$\sigma^s = -\frac{\theta - \theta_r}{\theta_s - \theta_r}(u_a - u_w) = -S_e(u_a - u_w) \quad [3.3]$$

where θ is the volumetric water content, θ_r is the residual volumetric water content, $\theta_s$is the saturated volumetric water content, S_e is the effective degree of saturation, and $u_w$is the pore-water pressure.

The matric suction values recorded at Q2 and Q6 are used along with Equation 3.2 to generate the suction stress time series from September 7, 2016 until November 27, 2017 (Figure 3.13). The saturated volumetric content (porosity) is taken as the highest value recorded by the sensors (0.39 m^3/m^3). Due to the process of sensor installation, the material surrounding the sensors is looser in nature and has a higher porosity than the embankment, which is about 0.2 m^3/m^3. The residual volumetric water content is obtained from the laboratory testing to be 0.10 m^3/m^3. The suction stress values at Q2 and Q6 are used along

with Equation 3.3 to generate the effective stress time series as shown in Figure 3.14. The total stress is calculated using the unit weight and the depth of the soil, which are 21.13 kN/m^3 and 0.91 m, respectively.

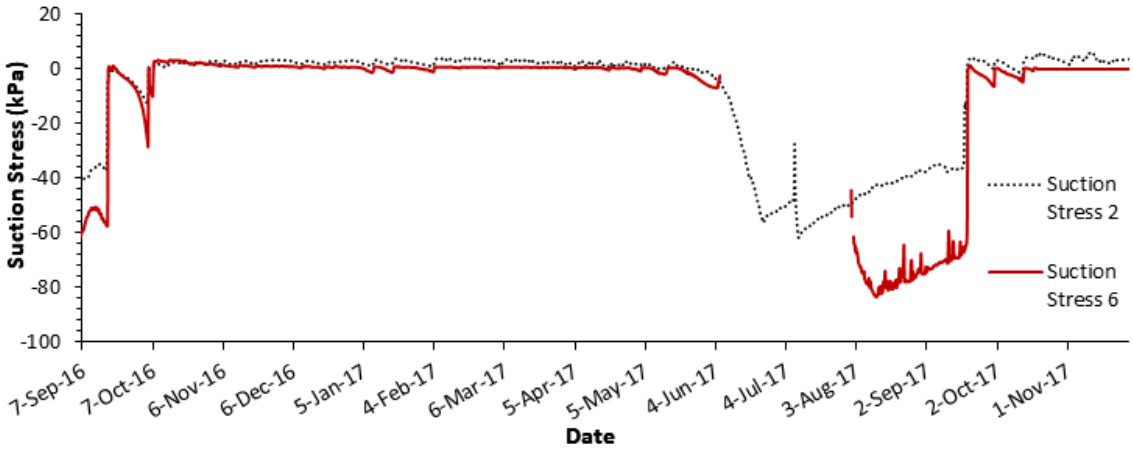

Figure 3.13 Suction Stress Time Series for Stations Q2 and Q6.

The results shown in Figures 3.13 and 3.14 reveal that the positive pore-water pressure in the beginning (from July 2015 to June 2016) generates a positive suction stress and, therefore, decreases or maintains a constant effective stress. In the first dry period, from June 2016 to the beginning of November 2016, the suction stress decreases substantially and, therefore, the effective stress increases from a value of approximately 20 kPa to 80 kPa. The effective stress quadrupled in magnitude, contributing to an increase in the shear strength of the soil. It should be noted here that in these calculations the total stress was assumed constant over the monitoring period. Both sensors showed a consistent response, given that they are located at similar depth from the ground surface.

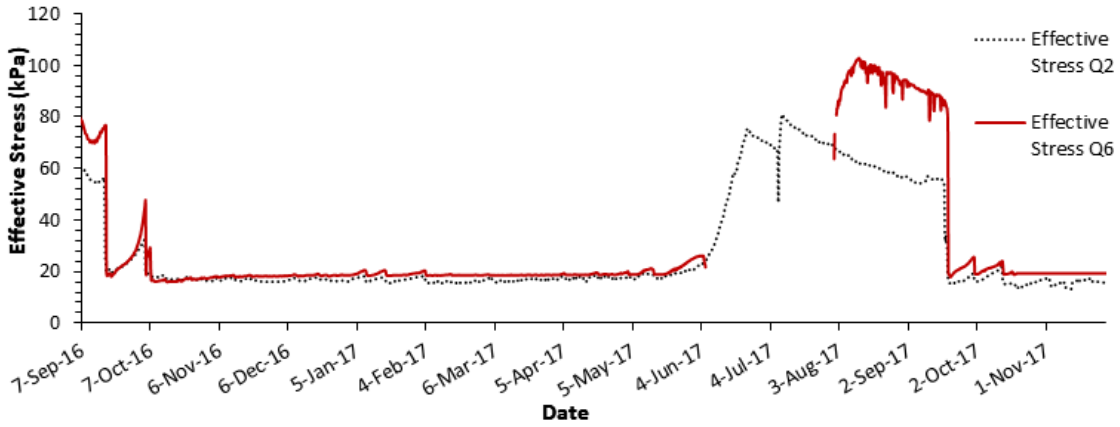

Figure 3.14 Effective Stress Time Series for Stations Q2 and Q6.

The same behavior was observed during the second dry period of June 2017 to the end of September 2017. In this event, Q2 showed similar stress values. However, Q6 showed lower suction stress and higher effective stress in comparison to the first dry event. This could be related to the fact that this second dry period contains more days of no rain, and Q6 is further downstream compared to Q2. The effective stress difference is about 20 kPa more than the first dry period.

3.4 Numerical Modeling of Transient Seepage

3.4.1 Model Setup

The commercial 2D finite element software package SEEP/W, 2018 (GEO-SLOPE International, Ltd 2018) was used to develop the numerical model. SEEP/W is a general seepage analysis program that can model saturated-unsaturated transient with land-atmospheric coupling at the ground surface. SEEP/W models unsaturated soils using the SWCC to predict the soil water content and corresponding suction under climate and tidal variations. As an initial attempt, a model time step of one month was set, but after looking

at the results, some of the initial values of the field data from the piezometer were still unstable and needed additional time to stabilize.

Figure 3.15 shows the geometry of the model used in the simulation. Table 3.2 presents the parameters used in the seepage analysis. For this study, a 15-month simulation period starting on September 7, 2016 and ending on November 27, 2017 was used. The starting date is when piezometer (Piezo4.75) was installed. The model uses the tidal variations and climate data from that period. The van Genuchten (1980) model is used to define the SWCC and HCF graphs.

The model has three zones composed of three materials. The foundation of the levee is a silt layer, which is assumed to be saturated at all times due to the high ground water table elevation. The silty sand layer, which comprises the levee embankment, is assumed to be the only layer that has variable saturation conditions depending on the hydraulic loading and climatic conditions. The gravel layer between the silt and silty sand is to represent the gravelly road section built to support the construction equipment, shown in Figure 3.10. The values of alpha (***a***), the slope of the SWCC (n), the compressibility (m_v), and the hydraulic conductivity (k) were varied only for the levee embankment (silty sand layer) to calibrate the model to the field measurements. Table 3.2 shows the soil properties that were used in the seepage analysis.

Table 3.2 Parameters used in the seepage analysis

Material	k_h (cm/s)	k_h/k_v	m_v (kPa^{-1})	θ_s	θ_r	*a* (kPa)	n
Silt	$10.0x10^{-6}$	1	$2.1x10^{-4}$	0.4	---	---	---
Silty Sand (embankment)	Varies	1	Varies	0.2	0.08	Varies	1.6

Gravel	10.0×10^{-8}	1	1×10^{-6}	0.3	---	---	---

3.4.2 Initial Conditions

The transient seepage model uses a steady state "parent". This steady state seepage analysis is used to predict the initial pore pressures/matric suctions and the piezometric surface for the levee cross section, as shown in Figure 3.16, for the transient seepage analyses. The upstream side was assigned a total head of 1.68 m, which reflects the water tide level on September 7, 2016. Also, the piezometer located in the core of the levee (piezo4.75) is assigned a total head of 1.46 m at the same time as the water tide boundary condition. The downstream toe is set to a total head of 0 m, which is the ground surface elevation. The bottom boundary of the model is set to a no flow condition. The K_y/K_x ratio was assumed to be 1.

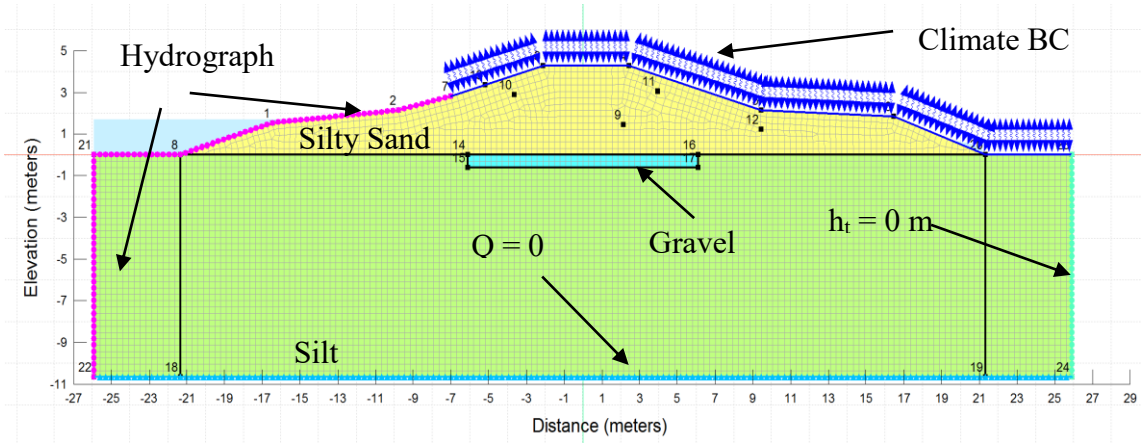

Figure 3.15 Geometry and Boundary Conditions of Numerical Model

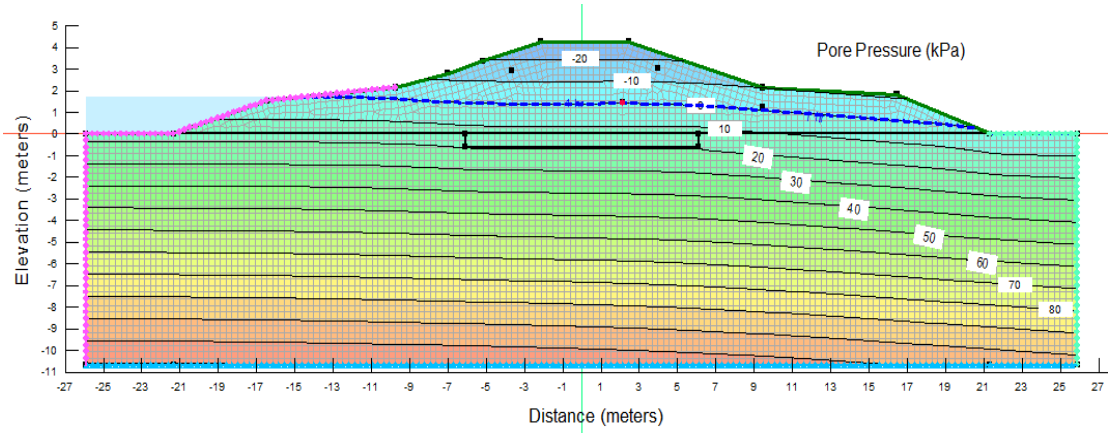

Figure 3.16 Initial Pore-Pressures Generated using Steady State Seepage Analysis

3.4.3 Transient Hydraulic Loading

The steady state seepage analysis provided the initial conditions of ground water pressures and defined a starting point for the transient seepage analysis. The boundary conditions applied in SEEP/W are shown in Figure 3.16. Similar to steady state, the bottom boundary condition is a no-flow boundary via a zero-unit flux condition.

Figure 3.9 shows the levee hydrograph from September 2016 to November 2017. The 6-hour data and 24- hour data is shown in the figure. The 24-hour data is presented as a clearer trend line of the water tide. As observed in Figure 3.9, the water tide cycled every 5-9 days, with a maximum of 2.5-m and a minimum of 1-m total head. The 6-hour data was used in this study as a hydraulic boundary condition. Climatic data including precipitation, temperature, wind speed, relative humidity, and net solar radiation were used as land-climate boundary conditions as described in the following section. The pore-water pressure generated by the transient seepage analysis was used to calibrate the model

parameters based on measured data from piezometer (Piezo4.75) and tensiometers at Q2, Q5, and Q6.

3.5 Calibration of Numerical Model

In an unsaturated transient seepage analysis, four soil properties are important: the SWCC properties (θ_s, θ_r, a, and n), the hydraulic conductivity in the x-direction (k_h), soil compressibility (m_v), and the initial conditions (Stark et al., 2017). The foundation silt and gravel layers were modeled as saturated-only materials, and the properties were obtained from field testing during construction. For the silty sand layer, the properties were obtained from TRIM testing as described above.

The model calibration process varied the van Genuchten curve fitting parameters, a and n along with the soil compressibility, m_v, and saturated hydraulic conductivity, k such that the model predicted pore-water pressures matched the measured data. Adjustments to the parameters to achieve accurate calibration was based on engineering judgment. The transient seepage model runs for about 10 months (7000 hours). The measured data from September 7, 2016 to July 7, 2017 were used for model calibration purposes. The meshing in this model used a four-node element composed of a square with over 7,011 elements.

Before starting the calibration, different boundary conditions were used to show the effect of each on the predicted pore-water pressures as discussed in the following section. The results presented in Figure 3.17a show the piezometer measured pore-water pressure compared to the model estimated pore-water pressure using variations in different boundary condition scenarios. These scenarios consisted of: considering the tide only, the tide plus the precipitation, and the tide plus climate boundary conditions (precipitation,

temperature, net radiation and wind speed). The same comparison is presented in Figure 3.17b, 3.17c, and 3.17d for the model predicted pore-water pressure with the measured data from tensiometers Q2, Q5, and Q6 located in other areas of the levee (Figure 3.2). The pore-water pressures were estimated from the field volumetric water content measured at Q2, Q5, and Q6 using Equation 3.4. These pore pressure data are plotted and added for comparison in Figure 3.17. Equation 3.4 can be used to estimate the pore-water pressure (matric suction) from a known volumetric water content using the van Genuchten (1980) model (Ellithy 2017):

$$\psi = a\left[\left(\frac{\theta-\theta_r}{\theta_s-\theta_r}\right)^{\frac{-1}{m}} - 1\right]^{\frac{1}{n}} \qquad [3.4]$$

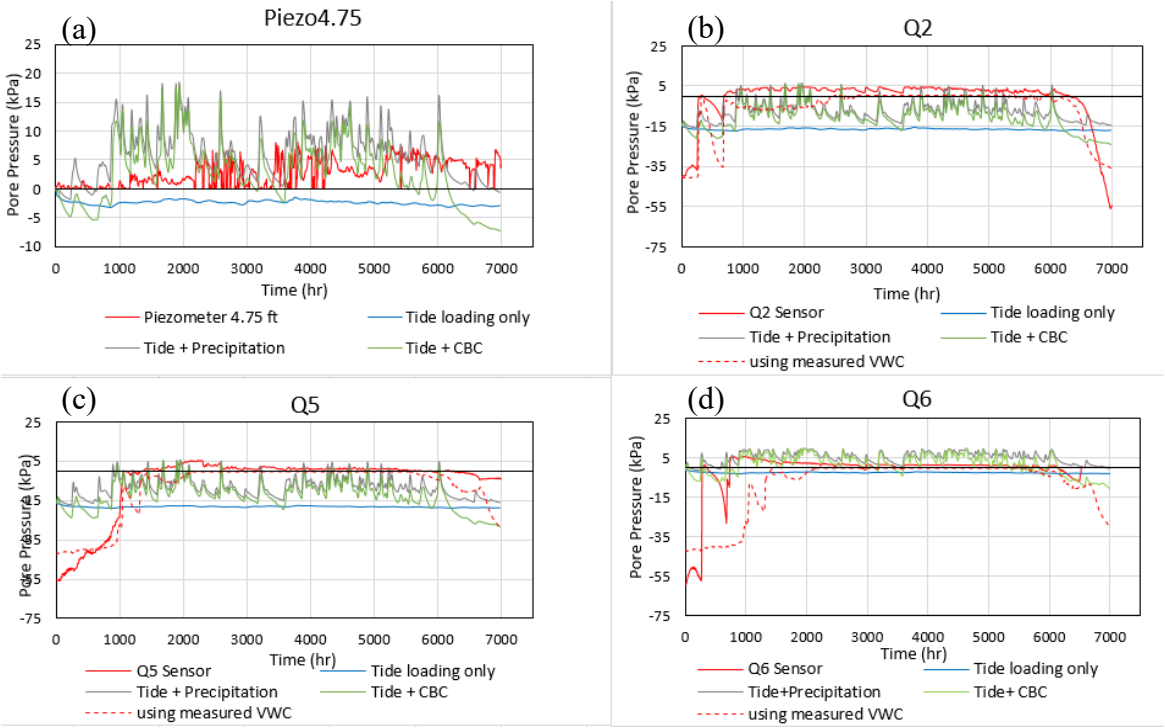

Figure 3.17 Effect of different boundary conditions for: a) piezometer4.75, b) tensiometer at Q2, c) tensiometer at Q5, and d) tensiometer at Q6 (from September 7, 2016 to July 7, 2017).

As shown in Figure 3.17, the inclusion of the precipitation, as well as the climate boundary conditions, resulted in pore-water pressure values closer to the measured than when considering tide loading only. Model results begin to conform to the field measurements after approximately three months (2000 hours). The piezometer (piezo4.75) was installed in the beginning of the modeling period, and it took this period to acclimate to the levee embankment conditions. Also, Figure 3.14 shows there was a dry event before the beginning of the modeling period, which resulted in an initially high matric suction measurements by the tensiometers. The model prediction did not match the tensiometer readings in the first 1000 hours (41 days), which was primarily the result of the selected initial pore-water pressure. However, the comparison between predicted and measured pore-water pressure improved significantly toward the latter part of the simulation. This emphasizes the importance of selecting the model duration period for calibration. Towards the end of the calibration period, there is a longer dry period, which resulted in a significant drop in the pore-water pressure in all monitored locations. The simulation starting time was set to the day piezometer was installed. It took about 2000 hours (82 days) until the piezometer reading acclimated to the surrounding soil at which point the measured and computed pore pressures agreed.

Tide+CBC was selected as the boundary condition for performing the calibration. In Figure 3.18, the average value of the van Genuchten fitting parameter n of 1.6) per TRIM results was used together with porosity θ_s and residual volumetric water content θ_r of 0.2 and 0.08, respectively. A saturated hydraulic conductivity k of $3e10^{-5}$ cm/s was used in the

model. Figure 3.18 provides a comparison of pore-water pressure generated from the model to measured values when changing the van Genuchten fitting parameter *a*.

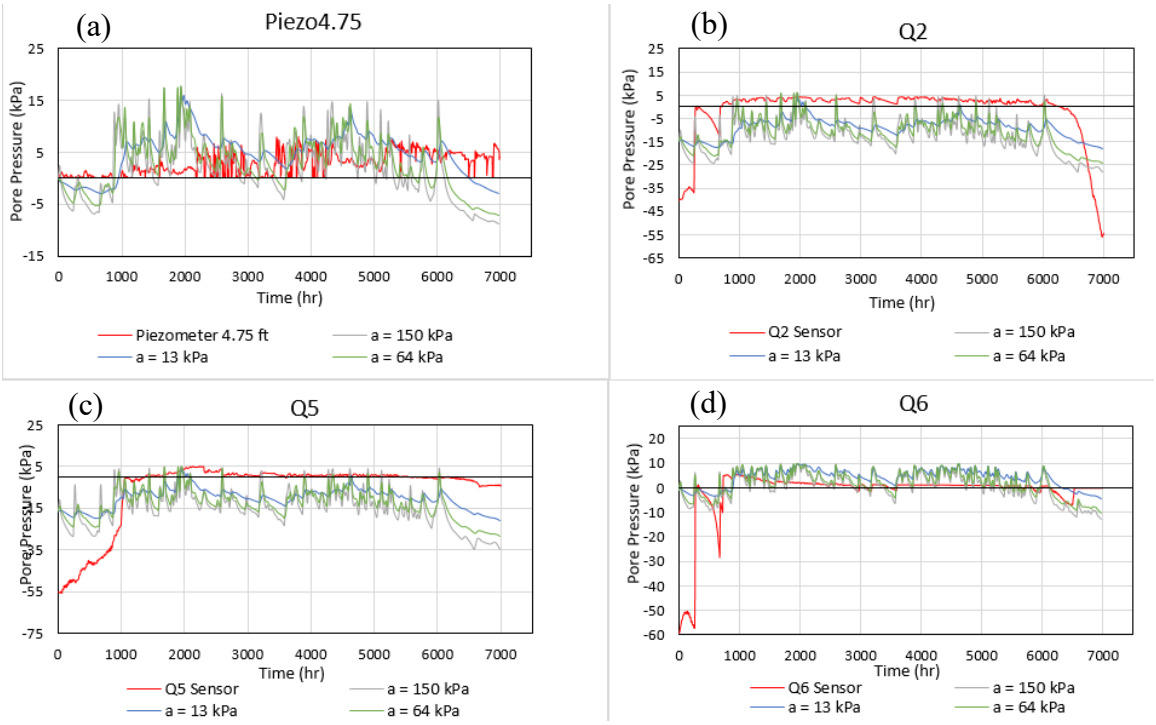

Figure 3.18 Effect of the van Genuchten (1980) parameter *a* for: a) piezometer, b) tensiometer at Q6, c) tensiometer at Q2, and d) tensiometer at Q5 (from September 7, 2016 to July 7, 2017).

As shown, the *a* parameter affects the estimated pore-water pressure. A value of *a* = 13 kPa seems to give a reasonable matching with the field measurements. Higher *a* values: 150 kPa and 64 kPa indicate a less drainable material results are below the measured most of the time. In general, the field measurements give higher matric suction values and higher positive pore-water pressure than predicted, in that they are more extreme than what the model predicts.

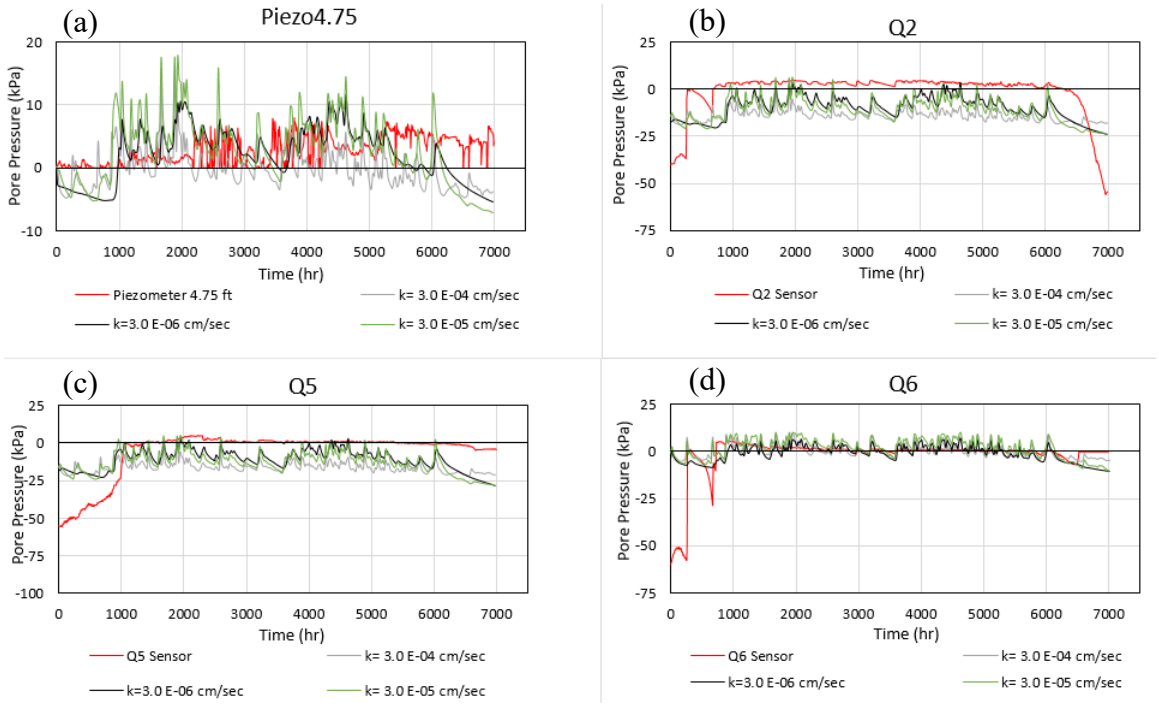

Figure 3.19 Effect of Hydraulic Conductivity for: a) piezometer, b) tensiometer at Q6, c) tensiometer at Q2, and d) tensiometer at Q5 (from September 7, 2016 to July 7, 2017).

Figure 3.19 shows the effect of the saturated hydraulic conductivity on the predicted pore-water pressures for Piezo 4.75, Q2, Q5, and Q6. The calibration showed no significant difference in predicted pore-water pressure. A value of $3x10^{-5}$ cm/s was selected to be used in the validation period, which is close to the measured value by TRIM.

3.6 Validation of Numerical Model

The model validation involves using the selected parameters from the calibration analysis during the initial period (0 to 7000 hours) to predict the measured field data during the following period (7000 to 10,704 hrs). The validation is done to ensure the model applicability.

Figure 3.20 shows the validation results for the selected parameters. The calibration results are also plotted for comparison purposes with the verification results. The validation process was performed from 7,000 hours to 10,704 hours (June 7, 2017 to November 27, 2017). The selected validation parameters are the following: a = 13 kPa, k =3x10^{-5} cm/s, n =1.6, and m_v = 2.09x10^{-5} 1/kPa. Figure 3.20a shows the verification for Piezo 4.75. The measured data shows a higher value than predicted by the model during the verification period. The model is considering the climatic condition for the dry period where the Piezo 4.75 does not read below zero and stays closer to the zero value. Figure 3.20b shows the model prediction matching with the measured pore-water pressure but with some time lag to match the peaks during the drought period. Figure 3.20c shows the model very close to the measured values obtained from sensor Q5. Figure 3.20d shows the model under-predicting the measured values from Q6. The high suctions measured by Q6 are possibly due to a drainage layer (gravel layer) under the sensor that may be draining the water away from the sensor. As a consequence, the soil around the sensor seems to have a very high suction during the dry period.

In general, the model predictions were found to closely match the measured data. From the measured data, the Piezo4.75 does not measure values below zero due to the sensor location, also, measured suction at Q6 location seem to be affected by a possible drainage layer below the sensor causing very high suctions values during the drought period. The model seems to match the trend and the approximate value of suction drop during dry period. However, measured suction shows a lag and sudden decrease trend over

a short period of time which is not matched by the gradual response of the model predicted PWP.

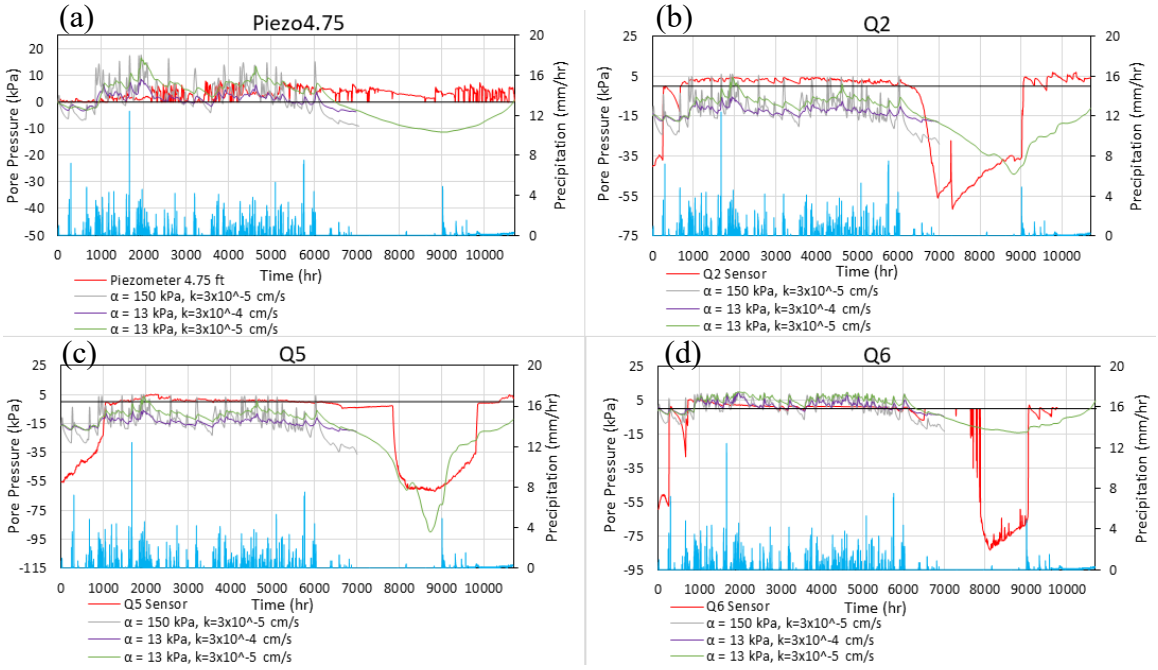

Figure 3.20 Model Validation Results (from June 7, 2017 to November 27, 2017).

3.7 Application: Modeling Levee Under a 100-Year Flood

The application of the calibrated model is illustrated by modeling the seepage and stability of the levee during a 100-year flood. Transient seepage analysis is first performed with the flood hydrograph. The pore pressure values obtained from the seepage analysis are then used in a set of limit-equilibrium analysis to obtain the factor of safety of the levee.

3.7.1 Transient Seepage Analysis

A Combined stage hydrograph model is a combination the data reported in Tetra Tech (2013) for Snohomish County and the FEMA Flood Maps. Tetra Tech (2013) resented a 100-year Stage Hydrograph for an area close to the site. Based on their

hydrographs, the time to peak does not change (62 hrs). Using the FEMA flood maps, we were able to get the peak stage for a 100-year event (2.68 m (8.8-feet NGVD29) = 3.81 m (12.5 –feet in NAVD88). Using the suggestions from Tetra Teach (2013) , 0.46 m (1.5-feet) was added to the 3.81 m (12.5-feet). A total of 4.27 m (14-feet) was used as the peak stage. The 0.46 m (1.5-feet) considers the backwater effect coming from the I5-Bridge.

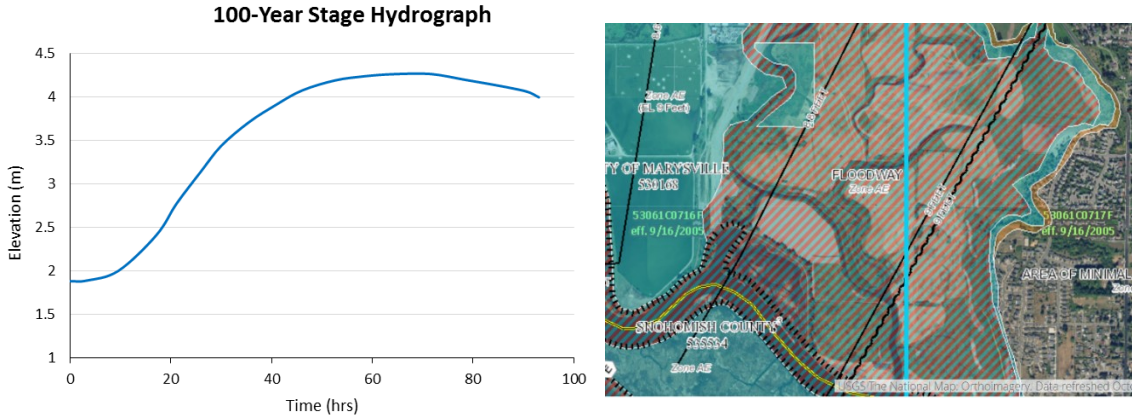

Figure 3.21 a) 100-year Flood Hydrograph, b) FEMA Flood Map 2005 for the Study Area (100-year flood).

The 100-year event hydrograph (Figure 3.21) brings the tide to an elevation of 4.25 m within 62 hrs. Whereas, the regular hydrograph used in the model has a high elevation 2.5 m. A 100-year precipitation depth of about 165 mm (6.5 in) was used for the event period, which was about 4 days.

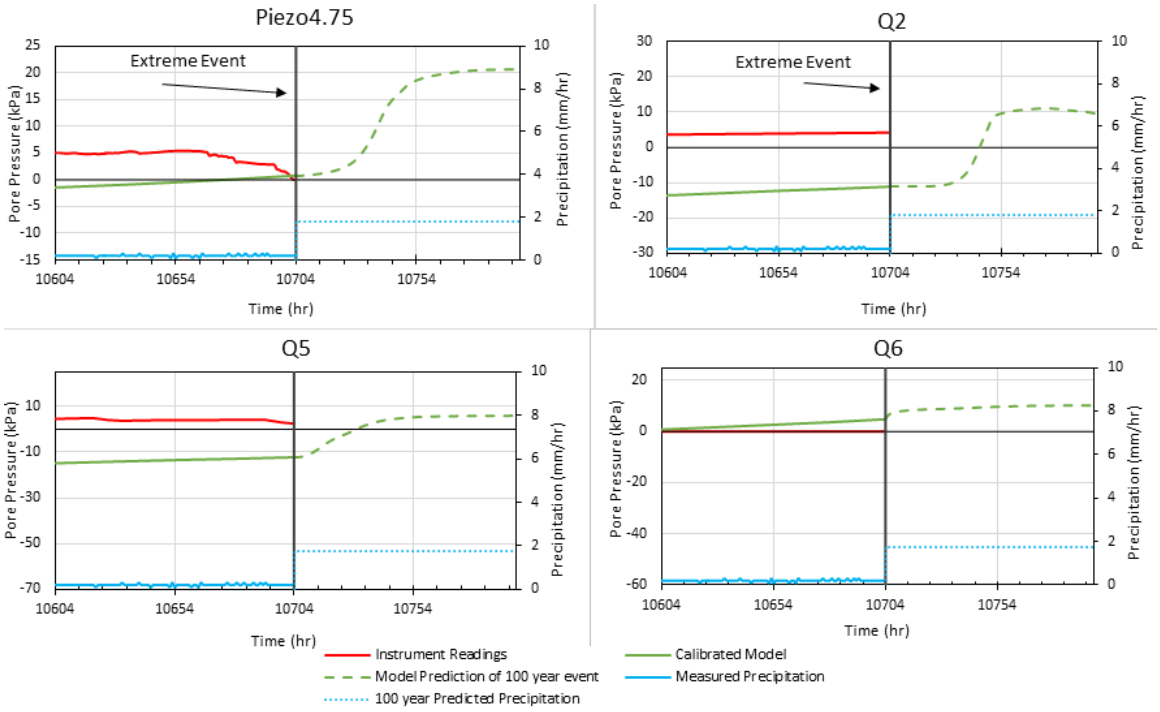

Figure 3.22 Predicted Pore Pressures Before and During Flood at Different Locations.

The 100-year event was started in the model right after the 15-month calibration and verification periods. A sudden increase in the pore-water pressure in all the monitored locations including the piezometer was observed. This increase is a result of the high 100-year event tide, which is in addition to a moderate precipitation of about 1.8 mm/hour for the duration of the event of 93-hours.

3.7.2 Stability Analysis

For this study, a limit-equilibrium slope stability model was built in SLOPE/W to analyze the stability of the levee upstream and downstream slopes under different conditions using Spencer method. For each condition, the pore-water pressure results were imported from the SEEP/W model and used in the stability analyses to determine the factor

of safety (FOS) The shear strength parameters for the three layers of the model used in the slope stability analysis are presented in Table 3.3.

Table 3.3 Slope stability parameters

Soil Property	Embankment Levee (SM)	Foundation (Silt)	Gravel
Unit weight (γ)	21.1 kN/m^3	18.1 kN/m^3	20.4 kN/m^3
Cohesion (c')	0 kPa	0 kPa / 21.5* kPa	0 kPa
Friction angle (ϕ')	38°	25°/ 0°*	32°

*Shear strength parameters used for undrained loading of the 100 year extreme event.

Figure 3.23 shows the variation of factor of safety for the entire modeling period for the upstream and downstream slopes. For the upstream slope, the factor of safety varies from 2.2 to 3. For the 100-year event, there is not a significant increase in factor of safety. For the downstream slope, the value of factor of safety up to 6,000 hrs varies during the wet period (winter period) from a value of 2.15 to 1.75. During the drought period, the value of factor of safety increases from 1.75 to 2.5. In general, the factor of safety increases for both slopes. The extreme event is plotted at the end of the modeling period, which produced a factor of safety of 1.55 for the downstream slope. The sudden increase in pore-water pressure in a short period of time during extreme 100-year event produced a substantial decrease in the factor of safety after a drought event. The upstream slope increases during the extreme event to a factor of safety of 3. The model seems to be successfully capturing the behavior of the levee during the extreme event modeled. This confirms the importance of incorporating the climatic conditions into the numerical models to represent the actual conditions during extreme events.

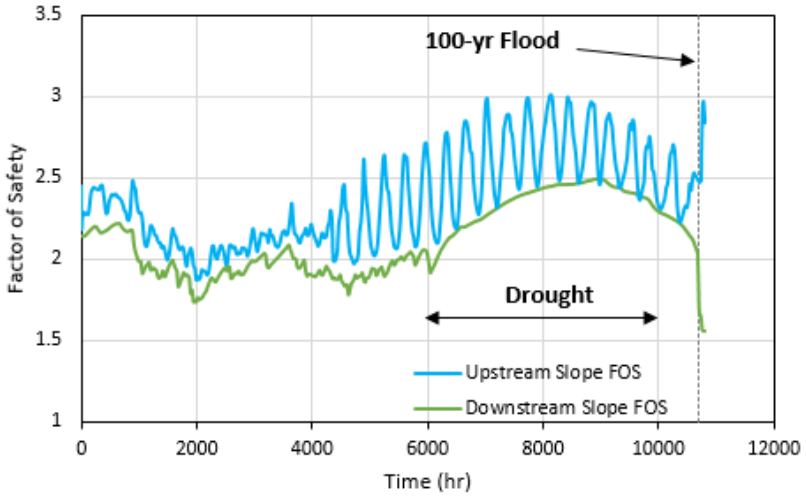

Figure 3.23 Factor of Safety for Upstream and Downstream Slopes.

CHAPTER IV

CONCLUSIONS

The main objective of this research was to improve the analysis of levees under transient seepage with the use of unsaturated soil mechanics. The work included a set of laboratory testing, field monitoring and numerical modeling performed to analyze a silty sand setback levee located near Seattle, WA. Soil samples taken from the site were used to perform index, water retention, and unsaturated multi-stage triaxial tests in the laboratory. A finite element model of transient seepage under saturated-unsaturated conditions was then developed and calibrated using the field data.

4.1 Summary and conclusions of work accomplished on single stage and multistage triaxial testing of a highly compacted silty sand

A series of unsaturated CD triaxial tests was carried out on high density compacted silty sand material retrieved from a setback levee in the Seattle area. The results presented in this paper showed that modified multistage unsaturated triaxial test procedures can be used to obtain the unsaturated shear strength parameters. This study demonstrate the possibility and convenience of performing unsaturated multi-stage triaxial testing on silty sand soils over the conventional triaxial testing. The comparison presented in this paper was based on a total of nine tests, five single stage triaxial tests compared to four multi-stage tests. The soils sample for all the tests were compacted to almost the same porosity

of 0.2. However, during consolidation and shearing at different confining pressures, the pore size distribution may have changed.

Unsaturated multistage test results showed that increasing the matric suction and the net confining pressure, the deviatoric stress and hence the shear strength increases. Increasing the matric suction results in an increment in effective stress, which confirms the increment in shear strength. For the saturated tests, the deviatoric stress were lower than the unsaturated tests. On the other hand, for unsaturated test at a constant matric suction, as the net confining pressure increases at the first stage, the axial strain decreases. On the second stage, the axial strain behaved randomly, either higher or lower than the second stage. It seems that the sample undergoes into a more plastic behavior after the first stage which results in reducing the axial strain at which the peak strength occurs in the following stage. For the ϕ^b parameter, the slope of each of the p'-q plots increases with the increase of matric suction. In conclusion, ϕ^b is not constant and decreases at higher matric suction. Also, the matric suction increases the slope of the stress versus strain curve, i.e. the modulus of elasticity increases. For a constant matric suction, the higher the net confining pressure results in a higher shear stress and axial strain. The comparison between single stage and multistage tests showed that for saturated tests the single stage is higher than multistage by 200 kPa, while for the unsaturated soil the single stage was less or equal to the multistage tests results. The volumetric strain results showed a variation in behavior which there is not a clear pattern on the volume change response. The peak state lines (PSL) obtained from the p'-q plots using the MIT formula showed that as you increase the matric suction the slope of p'-q increases and did not follow the saturated peak state line.

A methodology is presented for standardizing the multistage stage testing for unsaturated soils to be used by the advanced geotechnical laboratories. It is demonstrated that using multistage testing for unsaturated soils is a cost-effective alternative comparing it with the conventional single stage triaxial tests of unsaturated specimens. This method is not only economically feasible over the single stage, because the test time is shorter than the conventional, but also the error is significantly reduced by using just one sample during the manual preparations and during testing of the sample.

4.2 Summary and conclusions of work on integrating field monitoring and numerical analysis

The aim of this case study was to demonstrate how to effectively integrate field monitoring data and numerical analysis to better evaluate the performance of a levee during normal and extreme hydraulic loading conditions. The in situ data collected from an array of field instruments and a weather station were used along with a finite element model to study the response of a silty sand setback levee near Seattle under seasonal and tidal changes. The numerical model was calibrated and validated against field data. The calibrated model was used to simulate the evolution of pore pressure and factory of safety during a 100-year flood event.

Field measurements showed positive pore pressures during winter, which is considered the wet season for the area of study, and an increase in matric suction in drought events during the summer. It was found that including the precipitation as well as the other climatic boundary conditions such as temperature, solar radiation, humidity and wind speed, is essential for prediction of the pore-water pressures in the levee which resulted in a close match to the field measured values during the different seasons. Including only the

precipitation as a boundary condition resulted in a close match during wet periods, however, in dry events, the drop in PWP could be matched when considering the climatic boundary conditions.

The pore-water pressure obtained from the model showed a gradual change in response to the wet and dry periods whereas the field instruments showed a more abrupt change. This change could possibly depend on where the instruments are installed. For example, the upper layers in the levee are more affected by the climatic variations; while the lower layers are more affected by the piezometric line, which the model uses to estimate the pore-water pressures. Soil hydraulic conductivity anisotropy, looser soil density around sensors, or layers with higher hydraulic conductivity (none of which was considered in the model) could be contributing factors to less poorer agreement, especially in the cases where sudden drop in the pore-water pressure was observed.

4.3 Recommended Future Works

Based on the completed study and literature, the following areas of future research are recommended:

- Additional triaxial testing for clay material.
- Investigate changes in pore pressure and matric suction during drought and rainy seasons.
- Run numerical model for longer periods.
- Investigate the effect of volumetric strain on pore-water pressures in unsaturated soils.

REFERENCES

Allen, R. G., Walter, I. A., Elliott, R. L., Howell, T. A., Itenfisu, D., Jensen, M. E., & Snyder, R. L. (2005). The ASCE standardized reference evapotranspiration equation. 2005. Technical Committee report to the Environmental and Water Resources Institute of the American Society of Civil Engineers from the Task Committee on Standardization of Reference Evapotranspiration, ASCE.

Allen, R.G., M. Smith, L.S. Pereira and A. Perrier. (1994). "An update for the calculation of reference evapotranspiration." *ICID Bulletin*. 43(2):35-92.

Almahbobi, S & Tripathy, Snehasis & Cleall, Peter. (2018). Effects of confining stress and suction on volume change and shear strength behaviour of a collapsible soil.

Alonso, E., Jubert, E. & P. (2006). Weathering and degradation of shales: experimental observations and models of degradation. VI South American Rock Mechanics Conference, At Cartagena de Indias, Colombia

Anderson, A.C., NikiForoff, C.C, Leighty, W.J., Anderson, L.L., Hubbard, E.H., Maker, H.J., Olsen, H.A., Pasco R.E., and Waldo C.T. (1947). Soil Survey: Snohomish County Washington.

ASCE. (2017), "2017 Infrastructure Report Card." American Society of Civil Engineers, www.infrastructurereportcard.org.

Banerjee, A., Patil, U., Hoyos, L., and Bhaskar, P. (2018). "A Simplified Approach to Determine the Response of Unsaturated Soils Using Multistage Triaxial Test". International Foundations Congress and Equipment Expo (IFCEE).

Bishop, A. W. (1959). "The Principle of Effective Stress." Teknisk Ukeblad I Samarbeide Med Teknikk, 106(39), 859–863.

Bishop, A.W.T., Alpan, I., Blight, G.E., and Donald, I.B. (1960). "Factors controlling the strength of partly saturated cohesive soils." In: Proceedings of the Research Conference on Shear Strength of Cohesive Soils; University of Colorado. New York: A.S.C.E; 1961. 503-532.

Briaud, J-L, (2013). Geotechnical Engineering: Unsaturated and Saturated Soils, John Wiley & Sons.

Costa, Y. D., Cintra, J. C., and Zornberg, J. G. (2003). Influence of matric suction on the results of plate load tests performed on a lateritic soil deposit, Geotech. Test. J., 26, (2):219–227.

CRS, (2011). Locally Operated Levees: Issues and Federal Programs. Congressional Research Service (Available in: https://www.fas.org/sgp/crs/misc/R41752.pdf).

Ellithy, G. (2017). “A Spreadsheet for Estimating Soil Water Characteristic Curves (SWCC)”. ERDC Technical Note 17-1.

EM 1110-2-1901. (1993)."Seepage Analysis and Control for Dams". Department of the Army. U.S. Army Corps of Engineers. Washington, DC 20314-1000.

EM 1110-2-1913. (2000). "Design and Construction of Levees". Department of the Army. U.S. Army Corps of Engineers. Washington, DC 20314-1000.

Fredlund, D. G. and Rahardjo, H. (1993). Soil mechanics for unsaturated soil, New York, John Wiley & Son, Inc.

Fredlund, D. G., and Morgenstern, N. R. (1977). Stress state variables for unsaturated soils, Journal of Geotechnical Engineering Division, ASCE, Vol. 103, No. GT5, pp. 447–466.

Fredlund, D. G., Rahardjo, H., & Fredlund, M. D. (2012). Unsaturated Soil Mechanics in Engineering Practice. John Wiley & Sons.

Fredlund, D.G., Xing, A., and Huang, S. Y. (1994). “Predicting the permeability function for unsaturated soils using the soil-water characteristic curve,” *Canadian Geotechnical Journal*, 31(4), 533–546.

Freeze, R.A. (1971). Three-dimensional, transient, saturated-unsaturated flow in a groundwater basin. Water Resources Research, 7 (2), pp. 347-366.

Godt, J. W., Şener-Kaya, B., Lu, N., & Baum, R. L. (2012). “Stability of infinite slopes under transient partially saturated seepage conditions.” *Water Resources Research*, *48*(5). W05505.

Gulhati, S, and Satija, B.S. (1981). Shear strength of partially saturated soils /. Soil mechanics and foundation engineering. Proc. 10th international conference, Stockholm, June1981. Vol. 1, (A.A. Balkema). 1. 609-612.

Ho, D.Y.F. and Fredlund, D.G. (1982a). “A Multistage Triaxial Test for Unsaturated soils.” Geotechnical Testing Journal, GTJODJ, Vol. 5, No. ½, pp. 18-25.

Ho, D.Y.F., and Fredlund, D.G. (1982b). “Strain Rates for Unsaturated Soil Shear Strength Testing.” Proceedings of the Seventh Southeast Asian Geotechnical Conference, Hong Kong. Vol. 1. Pp. 787-803. November 22-26.

Inci, G., Yesiller, N., and Kagawa, T. (2003). Experimental investigation of dynamic response of compacted clayey soils, Geotech. Test. J., 26, (2), 125–141.

IPCC. (2013). Climate Change 2013: The Physical Science Basis. Contribution of Working Group I to the Fifth Assessment Report of the Intergovernmental Panel on Climate Change Cambridge University Press, Cambridge, United Kingdom and New York, NY, USA, 1535.

Jasim, F. H., Vahedifard, F., Ragno, E., AghaKouchak, A., Ellithy, G., (2017). "Effects of Climate Change on Fragility Curves of Earthen Levees Subjected to Extreme Precipitations." *Geo-Risk 2017: Geotechnical Risk from Theory to Practice*, GSP No. 285, June 4-6, 2017, Denver, CO, 498-507.

Khalili, N., and Zargarbashi, S. (2010). Influence of hydraulic hysteresis on effective stress in unsaturated soils. Géotechnique. Vol. 60, No. 9, 729-734.

Khosravi, A, Alsherif, N., Lynch, C and, McCartney J. (2011). Multistage Triaxial Testing to Estimate Effective Stress Relationships for Unsaturated Compacted Soils. Geotechnical Testing Journal. 35. 10.1520/GTJ103624.

Leong, E., Nyunt, T.T., and Rahardjo, H. (2013). Triaxial Testing of Unsaturated Soils. Springer Series in Geomechanics and Geoengineering. 3. 33-44. 10.1007/978-3-642-32492-5_3.

Leshchinsky, B., Vahedifard, F., Koo, H-B., and Kim, S-H., (2015). "Yumokjeong Landslide: An Investigation of Progressive Failure of a Hillslope using the Finite Element Method." *Landslides*, 12(5), 997-1005

Lu, N., and Likos, W. J. (2004). *Unsaturated Soil Mechanics*. Wiley, Wiley New York.

Lu, N., and Likos, W. J. (2006). Suction stress characteristic curve for unsaturated soils, J. Geotech. Geoenviron. Eng., 132, (2), 131–142.

Lu, N., Godt, J. W., and Wu, D. T. (2010). "A closed-form equation for effective stress in unsaturated soil." *Water Resour. Res*, 46(5), W05515.

METER Group Inc. (2018). Pullman, Washington. https://www.metergroup.com/

Ng, C. W. W., & Menzies, B. (2014). Advanced unsaturated soil mechanics and engineering. CRC Press.

NRC. (2012). Dam and Levee Safety and Community Resilience: A Vision for Future Practice. National Research Council. The National Academies Press, Washington, DC.

Oh, W. T., Vanapalli, S. K., and Puppala, A. J. (2009). Semi-empirical model for the prediction of modulus of elasticity for unsaturated soils, Can. Geotech. J., 46, (8), 903–914.

Patil, U., Puppala, A., Hoyos, L., and Banerjee, A. (2018). Strength, Stiffness and Radial Anisotropy of Compacted Silty Sand Under Suction-Controlled Axisymmetric Shearing. Geotechnical and Geological Engineering. pp 1-16.

Ragno, E., AghaKouchak, A., Love, C. A., Cheng, L., Vahedifard, F., Lima, C. H. R., (2018). "Quantifying Changes in Future Intensity-Duration-Frequency Curves Using Multi-Model Ensemble Simulations." *Water Resources Research*, 54(3), 1751-1764.

Rivera-Hernandez, X., Vahedifard, F., and Ellithy, G. (2017). Monitoring Suction Stress and Effective Stress in a Silty Sand Levee under Seasonal and Tidal Changes. PanAm-UNSAT 2017 Second Pan-American Conference on Unsaturated Soils.

Robinson, J. D., Vahedifard, F., and AghaKouchak, A. (2017). "Rainfall-triggered Slope Instabilities under a Changing Climate: Comparative Study using Historical and Projected Precipitation Extremes." *Canadian Geotechnical Journal*, 54(1), 117-127.

Salgado, R., Bandini, P., and Karim, A. (2000). Shear strength and stiffness of silty sand. J. Geotech. Geoenviron. Engng ASCE 126, No. 5, 451–462.

Satija, G.S. (1978). Shear Behavior of partially saturated soils. Ph.D. thesis, Indian Institute of Technology Delhi.

Seep/W. (2018). Geo-Slope International Ltd. [Computer Software].

Snohowish County. 2013. Appendix J Snohomish County Smith Island Estuarine Restoration Union Slough Hydraulic Model Study.

Stark, T. D., Jafari, N. H., Lopez-Zhindon, S., and Baghdady, A. (2017). "Unsaturated and transient 1038 seepage analysis of San Luis Dam," *J. Geotech. Geoenviron. Eng.*, 143(2), 04016093.

Tertra Tech (2013) Snohomish County, SMITH ISLAND ESTUARINE RESTORATION, UNION SLOUGH HYDRAULIC MODEL STUDY, Prepared for: Snohomish County Public Works Department Surface Water Management Division 3000 Rockefeller Avenue, MS-607 Everett WA 98201-4046, https://snohomishcountywa.gov/DocumentCenter/View/7374/Appendix-J?bidId=

USGCRP (U.S. Global Change Research Program). (2009). Global climate change impacts in the United States, Cambridge University Press, Washington, DC.

Vahedifard, F., AghaKouchak, A., Ragno, E., Shahrokhabadi, S., and Mallakpour, I. (2017a). "Lessons from the Oroville Dam." *Science*, 355(6330), 1139-1140.

Vahedifard, F., Mortezaei, K., Leshchinsky, B. A., Leshchinsky, D., and Lu, N. (2016b). "Role of suction stress on service state behavior of geosynthetic-reinforced soil structures." *Transportation Geotechnics*, 8, 45-56.

Vahedifard, F., Robinson, J. D., and AghaKouchak, A. (2016a). "Can Protracted Drought Undermine the Structural Integrity of California's Earthen Levees?" *J. Geotech. Geoenviron. Eng.*, 142(6), 02516001.

Vahedifard, F., Tehrani, F. S., Galavi, V., Ragno, E., and AghaKouchak, A. (2017b). "Resilience of MSE Walls with Marginal Backfill under a Changing Climate: Quantitative Assessment for Extreme Precipitation Events" *J. Geotech. Geoenviron. Eng.*, 143(9), 04017056.

Vahedifard, F., Williams, J. M., and AghaKouchak, A. (2018). "Geotechnical Engineering in the Face of Climate Change: Role of Multi-Physics Processes in Partially Saturated Soils." In *Proc. IFCEE 2018*, GSP No. 295, 353-364.

van Genuchten, M. T. Van. (1980). "A Closed-form Equation for Predicting the Hydraulic Conductivity of Unsaturated Soils." *Soil Science Society of America*, 44(5), 892-898.

Vanapalli, S. K., and Oh, W. T. (2010). A model for predicting the modulus of elasticity of unsaturated soils using the soil-water characteristic curve, Int. J. Geotech. Eng., 4, (4), 425–433.

Vanapelli, S. K., and Fredlund, D. G. (2000). "Comparison of different procedures to predict unsaturated soil shear strength." *Proc., Advances in Unsaturated Geotechnics*, GoeDenver 2000, Denver, Colorado, GSP No. 99, C. D. Shackelford, S. L. Houston, and N. Y. Chang, eds., ASCE, 195–209.

Wayllace, A., Lu, N., (2012). "A Transient Water Release and Imbibitions Method for Rapidly Measuring Wetting and Drying Soil Water Retention and Hydraulic Conductivity Functions," *Geotechnical Testing Journal*, 35(1), 103-117.

Yang, S. R., Huang, W. H., and Tai, Y. T. (2005). Variation of resilient modulus with soil suction for compacted subgrade soils. Transportation Research Record. 1913, Transportation Research Board, Washington, D.C., 99–106.

Yang, S. R., Lin, H. D., Kung, J. H. S., and Huang, W. H. (2008). Suction controlled laboratory test on resilient modulus of unsaturated compacted subgrade soils, J. Geotechnical. Geoenvironmental. Eng., 134, (9), 1375–1384.